

THE UNIVERSITY OF CALGARY

BENDING OF CABLES WITH INTERNAL FRICTION

BY

IRFAN S. ATATEKIN

A THESIS

SUBMITTED TO THE FACULTY OF GRADUATE STUDIES

IN PARTIAL FULFILLMENT OF THE REQUIREMENTS FOR THE

DEGREE OF MASTER OF SCIENCE

DEPARTMENT OF MECHANICAL ENGINEERING

CALGARY, ALBERTA

FEBRUARY 1984

© Irfan S. Atatekin 1984

THE UNIVERSITY OF CALGARY

FACULTY OF GRADUATE STUDIES

The undersigned certify that they have read, and recommend to the Faculty of Graduate Studies for acceptance, a thesis entitled "Bending of Cables with Internal Friction", submitted by Irfan S. Atatekin in partial fulfillment of the requirements for the degree of Master of Science.



Chairman, Dr. O. G. Vinogradov
Department of Mechanical Engineering



Dr. A. G. Doige
Department of Mechanical Engineering



Dr. S. Dost
Department of Mechanical Engineering



Dr. R. E. Loov
Department of Civil Engineering

February 1984

ABSTRACT

As the simplest model that approximates actual cable behaviour, a helical spring (coil) wound onto a cylindrical core is considered to analyze and explain the internal losses in the cables.

A section of the coil-core model is further isolated to investigate the formation of the slipping sections and the propagation of the slipping section boundaries along the cable.

It is shown that for a certain value of load, regions of complete slippage, partial slippage and complete non-slippage can be found inside the cable and the boundaries of these three regions are given by simple expressions. The resulting hysteresis loop is found to be in good agreement with the initial assumption of constant and uniformly distributed friction forces between the strands.

ACKNOWLEDGEMENTS

The author wishes to extend his most sincere appreciation and gratitude to Dr. Oleg G. Vinogradov, Professor of Mechanical Engineering, The University of Calgary, for his guidance, inspiration, kind advice and constructive discussions at every stage of this investigation.

Thanks are due to many of the technical staff members at the University of Calgary for their help in the successful completion of this project. In particular, the help rendered by Roy Bechtold, Art Moehrle and Nick Vogt must be mentioned.

Special thanks are certainly due also to Miss H. Kutluk for her cheerful and painstaking effort in typing the manuscript and to Miss Anita M. DeIure for taking time to edit what looked like an infinite number of pages.

The financial assistances of the National Research Council of Canada and of the Mechanical Engineering Department of the University of Calgary are greatly acknowledged.

This work is dedicated to my parents.

CONTENTS

| | Page |
|---|------|
| ABSTRACT | iii |
| ACKNOWLEDGEMENTS | iv |
| TABLE OF CONTENTS | vi |
| LIST OF TABLES | ix |
| LIST OF FIGURES | x |
| NOMENCLATURE | xi |
| | |
| CHAPTER 1 INTRODUCTION | 1 |
| | |
| CHAPTER 2 BENDING OF CYLINDRICAL HELICAL SPRING | 13 |
| 2.1 Introduction | 13 |
| 2.2 Spring Geometry and Internal Moments | 15 |
| 2.3. Deflection of a Spring Subjected to a Transverse Point Load | 21 |
| 2.4 Expression for the Deflected Center Line of a Spring | 26 |
| 2.5 Twisting of Coils | 30 |
| 2.6 Measurements of Free Rotations of a Spring at a X-Section | 33 |
| 2.7 Conclusion | 35 |

| | | |
|-----------|--|----|
| CHAPTER 3 | DERIVATION OF A HYSTERESIS LOOP AT A | |
| | CROSS-SECTION | 37 |
| 3.1 | Introduction | 37 |
| 3.2 | Twisting Mode of Coil Deformation | 40 |
| 3.2.1 | Stage One ($0 \leq \alpha \leq 1$) | 42 |
| 3.2.2 | Stage Two ($0 \leq \alpha \leq 1$) | 48 |
| 3.3 | Hysteresis Loop at a Cross-section | 52 |
| 3.4 | Coordinate Transformation for Second Stage | 53 |
| 3.5 | Experimental Results | 55 |
| 3.6 | Conclusion | 60 |
| CHAPTER 4 | GENERAL FORMULATION FOR CABLE GEOMETRY | 62 |
| 4.1 | Introduction | 62 |
| 4.2 | General Formulation for Cable Geometry | 64 |
| 4.3 | Boundary of the Slipping Sections | 67 |
| 4.4 | Change in the Moment of Inertia | 71 |
| 4.5 | Algorithm | 72 |
| 4.6 | Bending Energy Stored in the Cable | 81 |
| 4.7 | Conclusion | 84 |
| CHAPTER 5 | HYSTERESIS LOOP FOR A CABLE | 86 |
| 5.1 | Introduction | 86 |
| 5.2 | First Stage | 88 |
| 5.2.1 | Some Practical Applications | 98 |
| 5.3 | Second Stage | 99 |

| | | |
|---|--------------------------------------|-----|
| 5.4 | Comparison with Experimental Results | 106 |
| 5.5 | Internal Loss in a Cable | 109 |
| 5.6 | Conclusion | 118 |
| CHAPTER 6 GENERAL DISCUSSIONS AND CONCLUSIONS | | 121 |
| REFERENCES | | 128 |
| APPENDIX I | | 131 |
| APPENDIX II | | 132 |
| APPENDIX III | | 134 |
| APPENDIX IV | | 135 |

LIST OF TABLES

| Table | Title | Page |
|-------|---|------|
| I | Comparison of Theoretical and Experimental Values of Relative Rotation of Coils in a Spring | 34 |

LIST OF FIGURES

| Figure | | Page |
|--------|--|------|
| 1.1 | A Typical Stranded Conductor | 2 |
| 1.2 | A Typical ACSR Conductor | 3 |
| 2.1 | Physical Model of Coil-core System | 13 |
| 2.2 | Spring Geometry | 16 |
| 2.3 | Development of a Helix | 17 |
| 2.4 | Local Axes on a Helix | 21 |
| 2.5 | Lateral Spring Constant for Small Deflections | 25 |
| 2.6 | Distribution of Internal Torque Along the Helix | 32 |
| 2.7 | Rotation Angle of Free Coils Along the Helix | 33 |
| 3.1 | Basic Physical Model | 38 |
| 3.2 | Mathematically Equivalent Model to the Basic Element in Figure (3.1) | 39 |
| 3.3 | Slippage Along the Coil Section During Stage One | 47 |
| 3.4 | Slippage Along the Coil Section During Stage Two | 47 |
| 3.5 | Hysteresis Loop at a Cross-section | 54 |
| 3.6 | Experimental Set-up for Core-coil Model | 57 |
| 3.7 | Experimental Set-up for Measurements | 58 |
| 3.8 | Hysteresis Loops Obtained from | |

| | | |
|-----|--|-----|
| | Experiments | 59 |
| 4.1 | Numbering of Strands in a Cable | 64 |
| 4.2 | Boundary of the Slipping Sections | 68 |
| 4.3 | Slippage of Strands of a Cross-section | 74 |
| 4.4 | Change in the Stiffness of a Cable | 80 |
| 4.5 | Bending Energy Stored in a Cable | 82 |
| 5.1 | Theoretically Obtained Deflection Curve for a Cable | 97 |
| 5.2 | Deflection Curve for a Specific Case | 100 |
| 5.3 | Hysteresis Loop for a Cable | 104 |
| 5.4 | Hysteresis Loop for a Cable | 105 |
| 5.5 | Experimentally Found Hysteresis Loop | 107 |
| 5.6 | Energy Dissipated Per Cycle as a Function of Displacement | 110 |
| 5.7 | Comparison of Experimentally Found Energy Dissipation Curve | 113 |
| 5.8 | Loss v.s. Deflection Curve by Sturm | 114 |

NOMENCLATURE

Roman

- A Percent distance from the fixed end of the cable at which slippage in the cable ceases to exist
- A' $1 - A$
- B Percent distance from the fixed end of the cable at which total slippage at the cross-section ceases to exist
- B' $1 - B$
- C₁ A constant = 273.18
- C₂ As defined in equation (4.37.b)
- E Modulus of elasticity
- F Force
- G Modulus of elasticity in shear
- h Total length
- I Moment of Inertia of Cable cross-section
- I_e Equivalent moment of inertia of spring (equation 2.26)
- I_N Moment of Inertia for non-rotating cable cross-section
- I_R Moment of Inertia for completely-rotating cable cross-section

I_w Moment of Inertia of coil wire
 I_1 Moment of Inertia of coil wire w.r.t. normal axis
 I_2 Moment of Inertia of coil wire w.r.t. binormal axis
 i Unit vector in the direction of x-axis
 i Number of strands in each coil $0 \leq i \leq n$
 i_A Critical strand number after which strands do not slip
 i_B Critical strand number before which strands slip completely
 j Unit vector in the direction of y-axis
 K Number of strands in a cable
 k Unit vector in the direction of z-axis
 k' $h / 2 N$ (A constant)
 ℓ Length of the wire that spring is made of
 M Bending moment
 M_B Bending moment along the binormal axis (Figure 2.4)
 M_n Bending moment along the normal axis (Figure 2.4)
 M_t Torsional moment along the tangential axis (Figure 2.4)
 M_{ti} Torsional moment in the i 'th strand
 m_f Uniformly distributed friction torque
 N Total number of coils
 n Number of coils in a cable $0 \leq n \leq N$
 P Concentrated load

P_m Maximum value of load
 R Helix wire radius
 r A vector that describes any point on helix
 r Radius of the cylinder that helix is wound onto
 S As described in equation (3.9)
 s A variable along the coil $0 \leq s \leq l$
 T_i Net internal torque at any cross-section
 T_m As described in equation (3.6.b)
 T_m' As described in equation (3.13.b)
 T_{m_i} As described in equation (4.7.a)
 $T_{m'_i}$ As described in equation (4.7.b)
 $Text$ As described in equation (3.7)
 x_1 A'
 x_2 B'
 Y_m Non-dimensional displacement variable
 (equation 5.46)
 y Total displacement of the spring
 y_1 Displacement of spring under shear, displacement
 of the cable in the first stage of loading
 y_2 Displacement of spring under bending, displacement
 of the cable in the second stage of loading
 W Work done by applied load in the system
 z A variable along the coil or cable $0 \leq z \leq h$

Greek

- α Load coefficient $-1 \leq \alpha \leq 1$
- β A local variable
- β_1 Boundary of the slipping section in the first stage
- β_2 Boundary of the slipping section in the second stage
- β_{1i} Boundary of the slipping section in the first stage on the i 'th strand
- β_{2i} Boundary of the slipping section in the second stage on the i 'th strand
- γ As described in equation (3.13.b)
- Δ Increment, denotes incremental quantities
- ξ As described in equation (2.30.c)
- η Non-dimensional slippage angle
- η^* η after transformation
- η_1 Non-dimensional slippage angle in the first stage
- η_2 Non-dimensional slippage angle in the second stage
- η_{1m} Maximum value of η_1
- η_{2m} Maximum value of η_2
- θ_1 Rotation angle (slippage) in the first stage
- θ_2 Rotation angle (slippage) in the second stage
- κ Non-dimensional rotation angle
- λ Inclination of the coils w.r.t. x - y plane
i.e. helix angle

μ Poissons ratio
 Π As defined in equation (2.15)
 σ Angle between P and x-axis
 ϕ $\phi' - \phi_1$
 ϕ' Central angle of the helix
 ϕ_m Location of the center of the slipping section
after transformation
 ϕ_{mi} Location of the center of the slipping section
on i'th strand
 ϕ_{oi} Initial angle of i'th strand
 ϕ Central angle between the clamped end of the helix
and the x-axis
 Ψ Energy dissipated per cycle
 Ω Non-dimensional load coefficient as described in
equation (3.12)
 Ω_i Non dimensional load coefficient on i' th strand
 Ω_m Maximum value of Ω
 Ω_0 Value of Ω at the first strand of the first coil

CHAPTER ONE

INTRODUCTION

Strings, hanging chains and cables have been analyzed for centuries. Not only has cable behaviour been of interest because it has many applications but also because of the fundamental nature of problem solution. The catenary and vibrating string problems can be found in most elementary texts of mechanics and engineering mathematics.

During the late 1960's cables were studied with regard to both application and analysis. Cable systems were being considered as structural components in three dimensional networks; the cable supported roof used in the Munich Olympics in 1972 and the 1983 Saddledome in Calgary, are only but two examples. Ocean requirements in both private and military sectors placed greater emphasis on complex cable systems for mooring and undersea structures. The complexity of these applications overextended the classical approaches for analyzing such cable systems. Specifically, the catenary solution was difficult to apply to highly branched networks under transient loading [22]. In the design, operation, and expansion of electrical power systems it became necessary to know the physical

characteristics of conductors used in the construction of aerial distribution and transmission lines.

A typical stranded conductor made from bare copper (Figure 1.1) is very similar in geometry and design to the structural cables made from various alloys of steel.

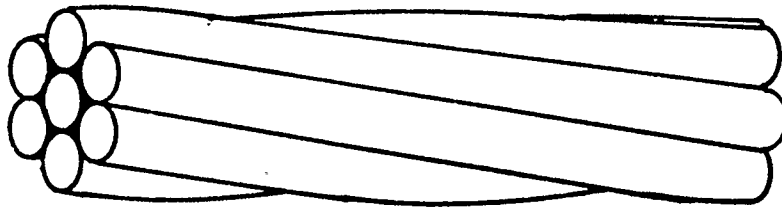


Figure (1.1) A Typical Stranded Conductor.

In the electric-power field the following types of conductors are generally used for high-voltage power transmission lines: stranded copper conductors, hollow copper conductors and ACSR (aluminum cable, steel reinforced). A stranded conductor is easier to handle and is more flexible than a solid conductor, particularly in the larger sizes. A typical ACSR conductor is illustrated in Figure (1.2).

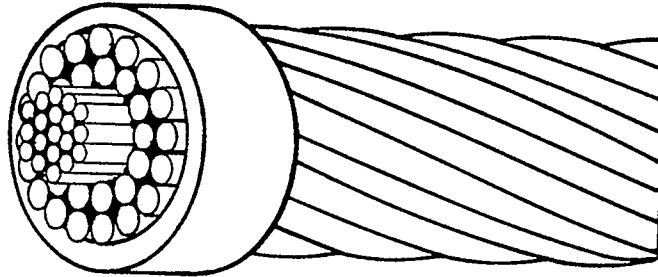


Figure (1.2) A Typical ACSR Conductor.

In this type of conductor, aluminum strands are wound around a core of stranded steel. Varying relationships between tensile strength and current-carrying capacity as well as overall size of conductor can be obtained by varying the proportions of steel and aluminum. By the use of a filler, such as paper, between the outer aluminum strands and the inner steel strands, a conductor of large diameter can be obtained for use in high voltage lines [13].

The effect of wind in producing vibrations in stranded cables has been known for many years, and the number of laboratory and field investigations and of reports on the subject has been continuously increasing as a consequence of general interest in the matter. The urgent necessity of

finding some practical solutions for the ever increasing number of transmission line failures has often led to the confusion between the causes and the consequences of the vibrations. Wind is the cause of the cable vibrations and cable vibrations in turn are the cause of strand strains that lead to the strand fatigue failures. Fatigue occurs almost entirely, 99 % or more, at hardware locations with the major portion of failures occurring at suspension clamps. However, a significant number of failures also occur at hot-line taps, spacers, dampers, aircraft warning devices, and dead ends, since the state of stress is similar to that at a suspension point. The lack of fatigue in free-span locations away from hardware is attributed to the fact that high dynamic strains occur only at restrained nodes [5], [7]. The data collected by Claren and Diana [7] shows dynamic stresses to be four times greater at the fixed support, or completely restrained node, than the free span maximum.

For a better understanding of cable mechanics a number of studies have been done to find the response of a cable subjected to various forms of loadings. Since cables are widely used for transmitting forces, most of the publications deal with the response of cables to axial loading and axial torsion [2], [4], [9], [10], [12], [14], [25]. In those papers, linear and non-linear analysis are

made to find the contact stresses between individual strands and on the core, and to evaluate the effective modulus for twisting and to determine the strains for the case of small and large deflections. Among these, work done by Huang [10] deals with finite extension of an elastic strand with a central core surrounded by a single layer of helical wires and subjected to axial forces and twisting moments. The theory of slender curved rods is used in the analysis and some geometrical non-linearities are considered. It is found that as a result of the contact between the central core and helical wires, a separation between helical wires can occur during the extension of the strand. In an early paper by Phillips and Costello [9], the method of separating the cable into thin wires and solving the general non-linear equations for bending and twisting of a thin rod subjected to line loads is used. Only axial force and axial twisting moment are considered and changes in helix angle and contact forces are calculated.

In another paper, taking advantage of geometric considerations, Machida and Durelli [4], give explicit expressions for the determination of axial force, bending and twisting moments in the helical wires, and for the axial force and twisting moment in the core of a 7-wire strand subjected to axial and torsional displacement.

Measurements on oversize epoxy models of the strand show good correlation with the theory and support the observation that axial load has no effect on the effective torsional rigidity of the strand. Costello and Miller [12] also analyze the effect of the twisting moments tending to unwind the strand compared to that of the same strand subjected to twisting that tends to tighten up the strand. Again in another paper by Costello and Phillips [9], effective modulus of twisted wire cables is considered. Six equilibrium equations are set and solved with simplifying assumptions. Costello and Phillips [14], in a later paper develop a more correct theory for twisted wire cables. Also, Costello [15] by using six equilibrium equations, finds the large deflections of helical spring due to bending moment. Picard's Method is used to obtain the solution and it is shown that the first approximation yields valid results for most practical cases.

The response of stranded cables to exciting forces due to wind has been investigated both analytically and experimentally by Claren and Diana [5]. They have studied the problem by two approaches. In one approach, the damper is treated as an exciting force on the taut cable alone and in the other approach, it is treated as part of a dynamic system composed of the taut cable with one or more dampers. In another paper written by the same authors [7], the

correlation between the dynamic strains occurring in span and those occurring at the rigidly clamped extremities on vibrating taut circular beams is shown. It is also suggested that the wire slippage occurring on real loaded stranded cables will reduce the dynamic strains and contribute to the internal damping of the cable.

As dampers play an important role in reducing the level of vibrations and strains, an attempt is made by Dhotorad, Ganesan and Rao [8] to study the effects of the location of dampers on maximum strains produced in the cable. It is reported that dampers have appreciable effects at high wind speeds and it is recommended to use actual experimental values instead of approximate solutions. In all the literature available to us, especially the works of Claren and Diana [5], [7] and the others [6], [8] a macroscopic view of analysis is used. The cable is assumed to be a long, slender rod and corresponding resonance frequencies are found from known solutions. From these known solutions, kinetic and potential energies of a vibrating cable are found. By using either the decay method or the forced vibration method energy dissipated due to internal damping and the damping function corresponding to this dissipated energy are derived [5]. The equation of motion is set up by means of Lagrange's Equations and resonant frequencies are found

with about 5 % accuracy. This approach proves to be useful in calculating the right size and number of dampers for a particular power line. In another effort to determine the dynamic strain distribution [7], the cable is again modelled as a slender rod while strains for this case are found from known solutions and related to experimentally established values by means of so called "slippage coefficients".

From the tests made on the deflection of cables, it has been found that a hysteresis loop always occurs when a cable is deflected and the load removed. If the hysteresis characteristics for cables of the commercial sizes at various tensions were known, the maximum amplitudes of vibrations could be predicted quite definitely [20]. Furthermore, knowing the hysteresis characteristics of the damper cables, the effects of different sizes and shapes of damper weights on the efficiency of a damper on a given size conductor may be determined theoretically [20], [7]. In a paper by Dhotarad, Ganesan and Rao [8] the effect of Stockbridge Type Dampers near each end of the span for different cable lengths is analyzed. A comparative study of the maximum strains produced is made for various wind power input assumptions. In finding the natural frequency of the cable with a damper, internal damping of the cable is neglected.

In another paper by Carroll [21], the amount of energy absorbed from the wind by the vibrating conductor is measured by means of a coil in a magnetic field and it is shown that the energy absorbed is proportional to the amplitude. In a paper by Pipes [18], energy taken is assumed to be varying as the square of the amplitude and even though it is stated that interstrand friction has great influence in absorbing energy and in mitigating vibration, it is again neglected and only the effect of dampers is taken into account. In another paper by Wagner [6], experimental load-deflection curves are obtained for a few cables and it is observed that the equivalent bending stiffness is considerably less than that of a rigid cable and the difference is attributed to the slip between the strands of the cable. Again in a paper by Sturm [19] the "composite value" for the stiffness of a cable is measured and substituted into the theoretical formulas. Sturm [20] again clearly states that the information available at present is not sufficient to estimate the maximum amplitudes of vibration for commercial sizes of cables under field conditions. If the hysteresis characteristics for cables of commercial sizes at various tensions were known, the maximum amplitudes of vibration could be predicted quite definitely.

Although the above statement by Sturm was made in 1939, all the major papers published since then on the subject of maximum amplitudes of cable vibrations have employed a rather macroscopic point of view in dealing with the losses in the cables. They have all employed some experimentally found loss coefficients in the equations for the vibrations of rods [8], [19], [7], [5].

No publication analyzing the frictional losses in a cable from a microscopic point of view could be found in the literature available to the author of this thesis. In a few papers a statical analysis of cables is attempted by considering a cable as a collection of helical springs wound around a central core [3], [24], [25] but they fail to explore the cause, type and effects of the interstrand relative motion on the total response of the cable. In fact, the term "inter strand motion" or "loosening of the cable" is quite frequently used in most publications to explain the discrepancies between various theoretical and experimental values used in analyzing the vibration of cables.

In this thesis a simple three dimensional model for the cable is developed to explain the internal losses in the cables. Using this simplified model, the primary mode of interstrand friction responsible for the internal losses in cables is determined and the mechanism of the

interstrand sliding is investigated. As the simplest model that approximates actual cable behaviour, a helical spring wound onto a cylindrical core is considered (Figure 2.1), Vinogradov and Atatekin [28], [29]. A section of this simple model is further isolated from the main model and analyzed to better understand the actual microscopic deformations taking place during cyclic loading of cables. Theoretical findings will then be compared with experimental results and the parameters that play the most critical roles in frictional losses in cables will be discussed.

In Chapter Two the expression for the centerline of a helical spring subjected to a transverse point load is derived. The expression for the deflected centerline of a helical spring is then compared with that of the cylindrical core and it is shown that the rotation of helical coils is the primary form of relative motion out of two possible forms of relative motions (e.g. rotation and translation). An expression for free rotation of the coils is derived and is found to be in excellent agreement with the experimentally measured values of rotation.

In Chapter Three, a portion of a helical coil is isolated from the rest of the system and subjected to a typical loading that occurs during the transverse deflection of the system. A uniformly distributed friction

force is assumed and the expressions for the rotation of the isolated portion of coil are derived. Theoretical results are found to be qualitatively in good agreement with the experimental results.

In Chapter Four, the equations derived for a single coil in the previous chapters are transformed into a geometry of six helical coils around one central core. Expressions for the change in the moment of inertia of a cable as a result of slippage are derived. Response of a cable to a quasi-statically applied transverse concentrated load is found. Theoretically calculated load-deflection curve is found to be qualitatively in good agreement with the experimental results.

In Chapter Five the hysteresis loop for a cable with internal friction is obtained and results are in good qualitative agreement with the experimental results.

Chapter Six provides an overall evaluation of the main content of this thesis. The major contribution of the present work includes a model for the explanation of interstrand friction and slippage inside the cables.

CHAPTER TWO

BENDING OF CYLINDRICAL HELICAL SPRINGS

2.1 INTRODUCTION

As mentioned in the first chapter, the most simple model that has all the features of most cable geometries is a helical spring wound around a cylindrical core as shown in Figure (2.1).

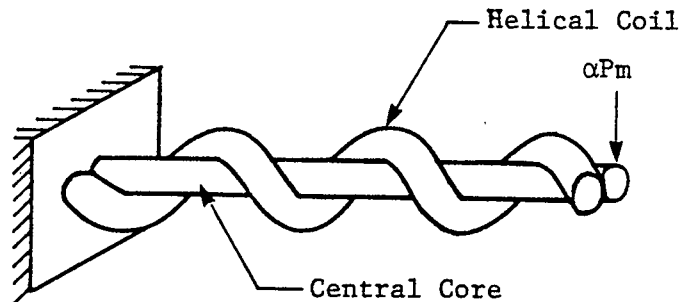


Figure (2.1) Physical Model of Coil-Core System.

It is then easy to postulate that there can be two types of relative motion between the helical spring and the cylinder inside it; a. lateral sliding of the coils on the cylinder, b. rotation of the coils, Vinogradov and

Atatekin [28], [29]. In a paper analyzing a helical tape on a cylinder subjected to bending [23] it is assumed that the surface of the cylinder and the tape centroidal axis undergo the same rotation. Considering the high flexibility of an elastic tape, it is a valid assumption. In our case, however, a helical spring with a much higher degree of rigidity is quite a different structure than the helical tape and requires some analysis before making any such assumptions.

For the model discussed above, clamped-free end conditions and a concentrated point load at the free end are assumed. The expression for the deflected centerline of a cylinder subjected to a transverse point load can be obtained from any strength of materials textbook. The case for a free* spring is quite different, however. In the literature, the response of a spring to axial load [2], [4], [10], to torsion [9], [11], [14], and to bending [15], [24] is analyzed. Despite all efforts, no publication about the response of a spring to transverse point load could be found. In a book by Andreeva [16], some empirical formulas are given to find the deflection of a spring at the point of application of load but nothing is said about the deflected center line.

* Free spring: A spring that does not have any friction force acting on its coils.

In an effort to find the solution for the deflected centerline of a spring subjected to a transverse point load, first, differential equations given by Love [1] are considered. Even after simplifications, the solution is rendered to six simultaneous non-linear differential equations. In pursuit of a simpler way of solution, an energy method similar to the one used by Prescott [2] is employed and results are presented.

2.2. SPRING GEOMETRY AND INTERNAL MOMENTS

As seen in Figure (2.2), the position vector connecting point of application of load to any point on the helix can be written as:

$$\underline{r} = -r \cos\phi' \underline{i} + r \sin\phi' \underline{j} - (k'\phi' - h)\underline{k} \quad (2.1)$$

where

r =radius of the cylinder that helix is wound onto,

ϕ' =central angle (e.g. for $\phi=2\pi$ helix makes one full turn),

ϕ_1 =central angle between the clamped end of the helix and x-axis,

$$\phi = \phi' - \phi_1$$

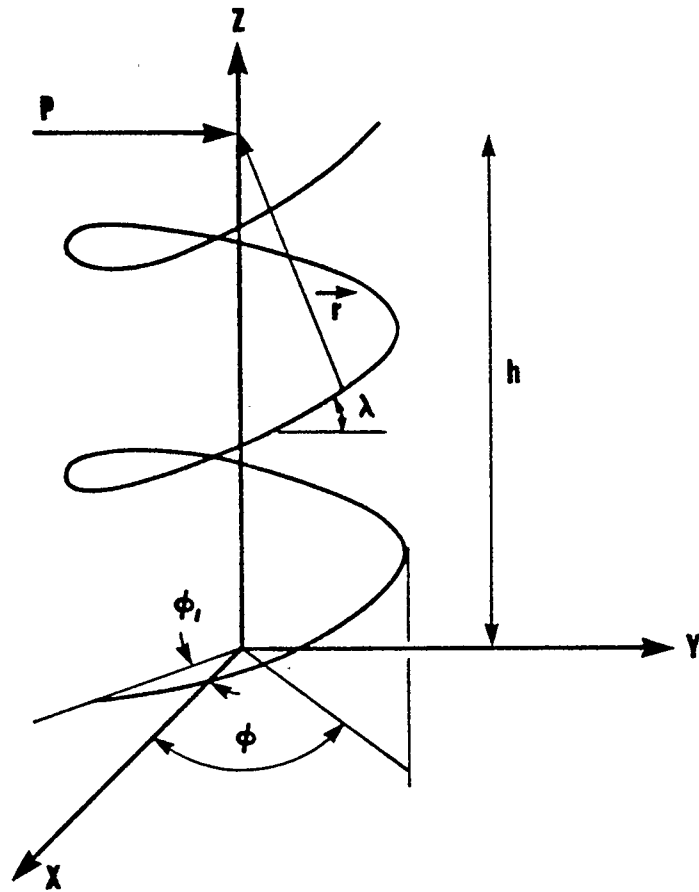


Figure (2.2) Spring Geometry.

λ =helix angle (inclination of the coils w.r.t. x-y plane. If $\lambda=0$ helix would be a circle),
 h =length of the spring,
 ℓ =length of the wire that spring is made of.

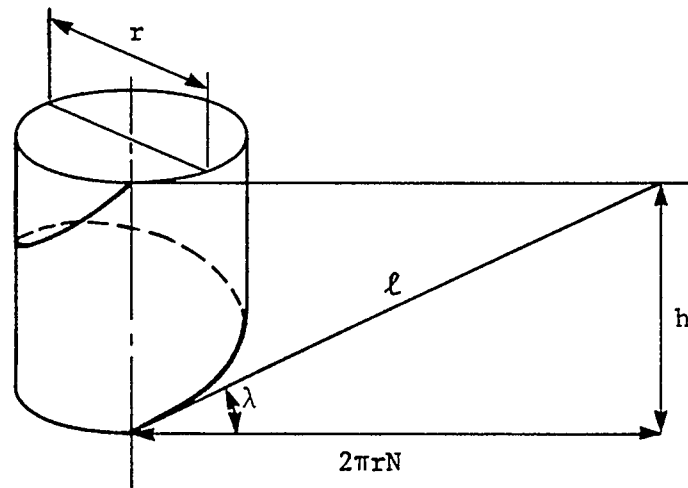


Figure (2.3) Development of a Helix.

Basically the following relationships hold between " ℓ ", " h " and " λ ":

$$\tan\lambda = \frac{h}{2\pi rN} \quad (2.2.a)$$

$$\sin\lambda = \frac{h}{\ell} \quad (2.2.b)$$

$$\cos\lambda = \frac{2\pi rN}{\ell} \quad (2.2.c)$$

where

N = Total number of coils.

By substituting "n" for "N" and "z" for "h" the following equations in terms of the variables z, n, and s can be obtained:

$$\tan\lambda = \frac{z}{2\pi r n} \quad \begin{array}{l} 0 < z < h \\ 0 < n < N \\ 0 < s < \ell \end{array} \quad (2.3.a)$$

$$\sin\lambda = \frac{z}{s} \quad (2.3.b)$$

$$\cos\lambda = \frac{2\pi r n}{z} \quad (2.3.c)$$

and,

$$\phi' = 2\pi n \quad (2.4)$$

The distance along the center line can be expressed as:

$$z = \frac{h}{2\pi r N} \phi' \quad (2.5)$$

or,

$$z = k' \phi' \quad (2.6)$$

where

$$k' = \frac{h}{2\pi N} = r \tan \lambda \quad (2.7)$$

Moment resulting from the concentrated load at the free end can be found from:

$$M = r_x F \quad (2.8)$$

where

$$F = P \cos \sigma \dot{i} + P \sin \sigma \dot{j} \quad (2.9)$$

then the moment at any cross section is found to be:

$$M = P \sin \sigma (k' \phi' - h) \dot{i} - P \cos \sigma (k' \phi' - h) \dot{j} + Pr (\sin \phi' \cos \sigma - \sin \sigma \cos \phi') \dot{k} \quad (2.10)$$

Since we are only interested in finding the deflected center line which does not change for any orientation of axes, a special orientation for helix and force is chosen to simplify the expressions as much as possible.

It is taken

$\sigma = 90$ (loading is in the same direction as
y-axis)

$\phi_1 = 0$ (helix starts at the x-axis)

Then the expression (2.10) can be written as

$$M = -P (k'\phi - h) \lambda - P r \cos\phi k \quad (2.11)$$

The above expression for moment, when decomposed along normal tangential and binormal axes takes the following forms:

$$M_n = P (k'\phi - h) \cos\phi \quad (2.12.a)$$

$$M_b = -Pr \cos\phi \cos\lambda - P (k'\phi - h) \sin\phi \sin\lambda \quad (2.12.b)$$

$$M_t = -Pr \cos\phi \sin\lambda + P (k'\phi - h) \sin\phi \cos\lambda \quad (2.12.c)$$

where

M_n = bending moment along the normal axis

M_b = bending moment along the binormal axis

M_t = torsional moment along the tangential axis.

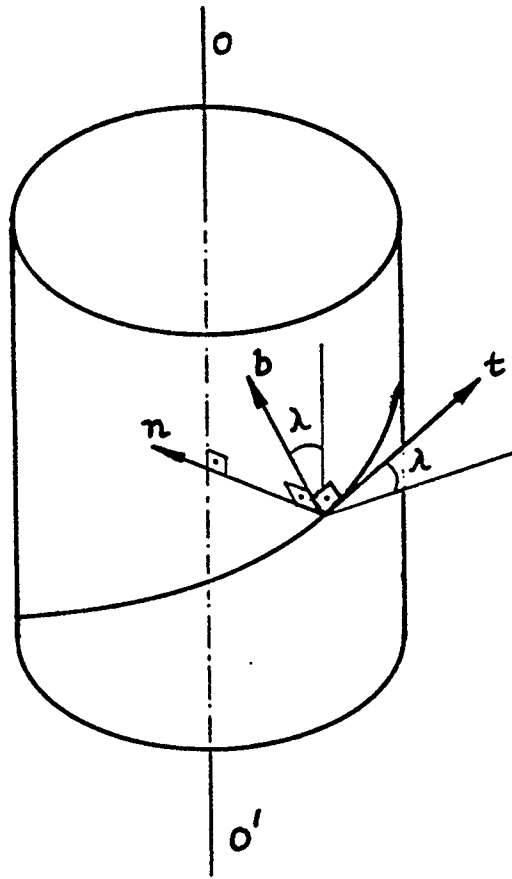


Figure (2.4) Local Axes on a Helix.

2.3. DEFLECTION OF A SPRING SUBJECTED TO A TRANSVERSE POINT LOAD

Since two bending moments and one torsional moment are in perpendicular planes (Equation 2.12) and their axes coincide with the positions assumed for the principal axes of the x-section, total energy can be written for the case of small strains as follows [2]:

$$W = \frac{1}{2} \int_0^{\ell} \frac{Mn^2}{EI_1} ds + \frac{1}{2} \int_0^{\ell} \frac{Mb^2}{EI_2} ds + \frac{1}{2} \int_0^{\ell} \frac{Mt^2}{GJ} ds \quad (2.13.a)$$

where

$$ds = r d\phi / \cos\lambda \quad (2.13.b)$$

If equation (2.12) is put into (2.13) and integrated the following expression can be obtained:

$$W = \frac{1}{2} P^2 \Pi \quad (2.14)$$

where

$$\begin{aligned} \Pi = & \frac{r \sec\lambda}{2 EI_1} \left(\frac{h^2 \ell}{r \sec\lambda} + \frac{8}{3} k'^2 N^3 \pi^3 - 4hk'N^2\pi^2 \right) \\ & + \frac{r \sec\lambda}{EI_2} \left(\frac{r^2 \cos^2\lambda \ell}{2 r \sec\lambda} + \frac{4}{3} k'^2 N^3 \pi^3 \sin^2\lambda - 2hk'N^2\pi^2 \sin^2\lambda \right. \\ & \left. + \frac{h^2 \ell \sin^2\lambda}{2 r \sec\lambda} \right) + \frac{r \sec\lambda}{GJ} \left(\frac{r^2 \sin^2\lambda \ell}{2 r \sec\lambda} + \frac{4}{3} k'^2 N^3 \pi^3 \cos^2\lambda \right. \\ & \left. - 2hk'N^2\pi^2 \cos^2\lambda + \frac{h^2 \ell \cos^2\lambda}{2 r \sec\lambda} \right) \end{aligned} \quad (2.15)$$

If "y" is the deflection of the point where the load is applied, work done can be written as follows:

$$W = \int_0^y P(y) dy \quad (2.16)$$

If equation (2.16) is equated to equation (2.14):

$$\int_0^{y_1} P(y) dy = \frac{P^2}{2} \Pi \quad (2.17)$$

since Π is a constant for a given geometry, differentiating both sides of equation (2.17) gives:

$$P = P \Pi \frac{dP}{dy} \quad (2.18)$$

or

$$\frac{dP}{dy} = \frac{1}{\Pi} \quad (2.19)$$

Since the right hand side of (2.19) is constant and $P = 0$ when $y = 0$, by integration it can be found that:

$$y_1 = \Pi P \quad (2.20)$$

If, now the expression for Π is substituted from equation (2.15) into equation (2.20), and by using the following identities:

$$I_1 = I_2 = I_w \quad (2.21.a)$$

$$J = 2I_w \quad (2.21.b)$$

$$G = \frac{E}{2(1+\mu)} \quad (2.21.c)$$

and equation (2.2), the following expression for the transverse deflection of a spring can be obtained:

$$y_1 = \frac{Pl}{2EI_w} \left\{ h^2(2+\mu \cos^2\lambda) + r^2(1+\mu \sin^2\lambda) - \frac{4}{3} \frac{Nh^2 r}{\ell \cos\lambda} (2+\mu \cos^2\lambda) \right\} \quad (2.22)$$

It should be noted, however, equation (2.22) gives the deflection of a spring only at the point of application of load. Before pursuing the matter any further to obtain an

expression for the deflected center line, it should prove useful to check the expression derived with those found in the literature.

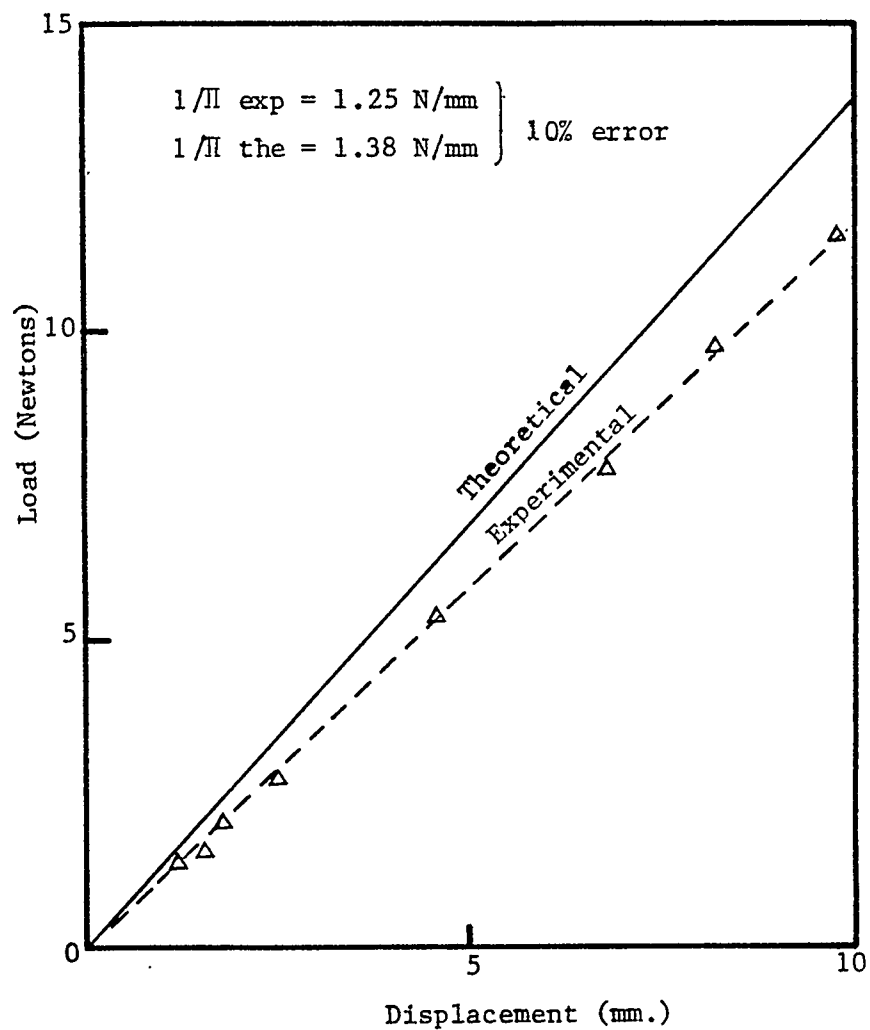


Figure (2.5) Lateral Spring Constant for Small Deflections.

The only other expression that could be found is supplied by Andreeva [16]; however no derivation is shown, and the equation is supplied in terms of two coefficients (see Appendix I). Although it could not be proved analytically that the expression supplied by Andreeva is equal to equation (2.22), nonetheless, excellent agreement is obtained in terms of numerical results.

To further check the theoretical results experimentally, an auto shock spring was tested (Appendix IV). Because of the rather large tolerances used in the auto industry, the spring used for experiments had rather large variations of helix angle and internal diameter. The experimental deflection curve obtained, however, is still in good agreement with the theoretical one with only 10 % error as seen in Figure (2.5).

2.4. EXPRESSION FOR THE DEFLECTED CENTER LINE OF A SPRING

The force and moment at any cross-section "z" of a spring resulting from an applied load at the free end can be written as follows:

$$\text{Force} = P \qquad (2.23.a)$$

$$\text{Moment} = P (h-z) \quad (2.23.b)$$

Therefore the displacement at any cross section "z" resulting from the force at any cross section "z" can be written from equation (2.22) by substituting "z" for "h":

$$y_1 = \frac{Ps}{2EI_w} \{z^2 (2+\mu \cos^2\lambda) + r^2 (1+\mu \sin^2\lambda) - \frac{4}{3} \frac{\pi N z^2 r}{s \cos\lambda} (2+\mu \cos^2\lambda)\} \quad (2.24)$$

The expression for the curvature of a spring under pure bending moment is given by Timoshenko [3] as:

$$y_2 = \frac{M z^2}{2 EI_e} \quad (2.25)$$

where

$$I_e = \frac{2 I_w \sin\lambda}{2+\mu \cos^2\lambda} \quad (2.26)$$

If the expression for bending moment at any cross-section resulting from the point applied load is

substituted into the equation (2.25), expression for the displacement under bending load is obtained:

$$y_2 = \frac{P (h-z) z^2}{2 E I e} \quad (2.27)$$

Assuming small displacements, expression for the deflection of a spring at any cross-section under applied point load can be obtained follows:

$$y = y_1 + y_2 \quad (2.28)$$

or

$$y = \frac{P s}{2 E I} [z^2 (2+\mu \cos^2 \lambda) + r^2 (1+\mu \sin^2 \lambda) - \frac{4}{3} \frac{N z^2 r}{s \cos \lambda} (2+\mu \cos^2 \lambda)] + \frac{P z^2 (h-z)}{4 E I \sin \lambda} (2+\mu \cos^2 \lambda) \quad (2.29)$$

or by using equation (2.3), it can be rearranged as follows:

$$y = \frac{P}{E I e} [z^3 (-\frac{1}{6} + \xi) + \frac{z^2 h}{2}] \quad (2.30.a)$$

where

$$I_e = \frac{2 I_w \sin \lambda}{(2 + \mu \cos^2 \lambda)} \quad (2.30.b)$$

$$\xi = \frac{(1 + \mu \sin^2 \lambda)}{4\pi^2 N^2 \tan^2 \lambda (2 + \mu \cos^2 \lambda)} \quad (2.30.c)$$

Referring to the equation of deflection for a beam
[17]:

$$y = \frac{P}{EI} \left[z^3 \left(-\frac{1}{6} \right) + \frac{z^2 h}{2} \right] \quad (2.31)$$

By comparing equations (2.30.a) and (2.31) the discrepancy associated with the term ξ in equation (2.30.a) can be seen. It means that both core and coil slide with respect to each other in a longitudinal direction. However, a simple estimation shows that the discrepancy is negligible in the case of cables. Indeed, in applications the lead angle $\lambda > \pi/4$, which means that $\xi < 0.025/n^2$ and can be neglected compared with $1/6$ even for the first coil turn. It may be concluded that the bending type of coil deformation is not essential in the analysis of frictional losses.

It should also be noted that this is the first time an equivalent bending stiffness for springs under point load is derived and is shown to be similar to the one given by Timoshenko [3] for pure bending.

2.5. TWISTING OF COILS

Since it is found that the rotation of coils in a cable is the primary form of energy dissipation; as a first step in further analysis, "free" rotation of coils is considered.

The expression for torsional moment at any cross-section was found to be :

$$M_t = -Pr \cos\phi \sin\lambda + P(k'\phi - h) \sin\phi \cos\lambda \quad (2.32)$$

Using equations (2.7) for k' and (2.2.a) for h , equation (2.32) can be reduced to the following form:

$$M_t = -Pr \sin\lambda [\cos\phi - (\phi - 2\pi N) \sin\phi] \quad (2.33)$$

and the expression for rotation angle can be found as:

$$\theta_f = \frac{1}{G J_0} \int_0^{\theta} M_t(\phi) d\lambda \quad (2.34)$$

and in terms of a unit vector:

$$M_t(\phi) = M_t(\phi) \frac{d\mathbf{u}}{|d\mathbf{u}|} \quad (2.35)$$

and

$$\mathbf{u} = r \cos\phi \mathbf{i} + r \sin\phi \mathbf{j} + r \tan\lambda \mathbf{k} \quad (2.36)$$

if differentiated,

$$d\mathbf{u} = (-r \sin\phi \mathbf{i} + r \cos\phi \mathbf{j} + r \tan\lambda \mathbf{k}) d\phi \quad (2.37)$$

If equation (2.37) is put into equations (2.35) and (2.34) and by using the identity:

$$(1 + \tan^2\lambda) = \frac{1}{\cos^2\lambda}$$

the following expression for the rotation angle can be obtained:

$$\theta_f = \frac{Pr^2 \sin\lambda}{GJ \cos\lambda} [\cos\phi (\phi - 2\pi N) + 2\pi N] \quad (2.38)$$

or in terms of non-dimensional quantities:

$$\kappa = \cos\phi (\phi - 2\pi N) + 2\pi N \quad (2.39.a)$$

where

$$\kappa = \frac{GJ}{Pr^2 \tan\lambda} \quad (2.39.b)$$

As can be seen from equation (2.39) the dimensionless parameter κ is only dependent on the maximum number of coils and does not depend on load or any other spring parameters.

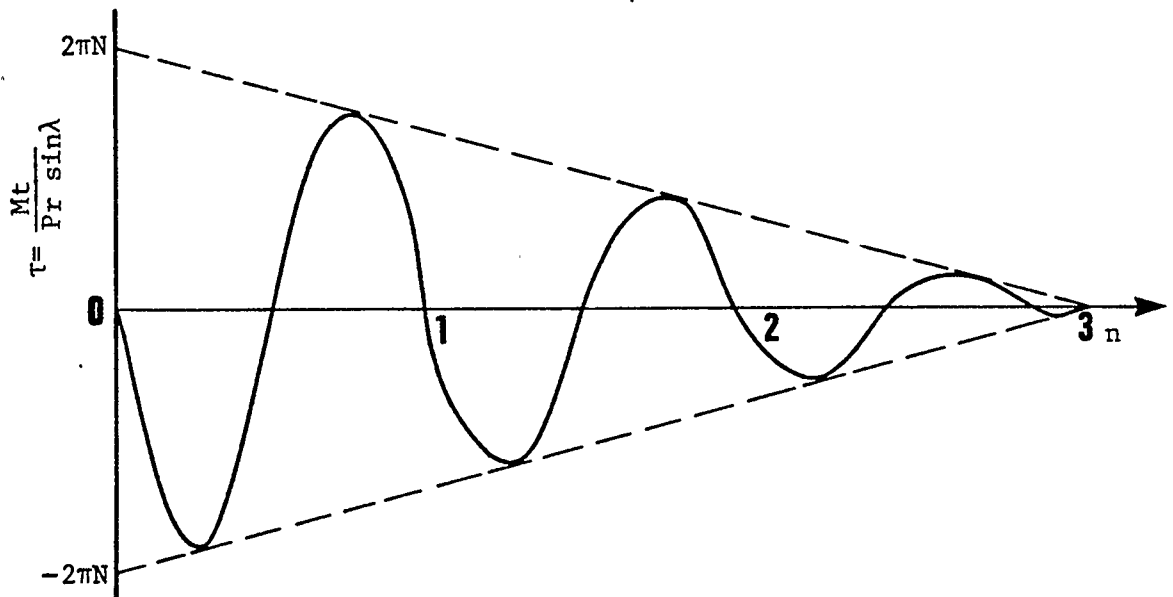


Figure (2.6) Distribution of Internal Torque
Along the Helix.

2.6. MEASUREMENT OF FREE ROTATIONS OF A SPRING AT A CROSS-SECTION

After deriving the expressions for free rotation of coils of a spring, it became desirable to develop a device for measuring the rotation at a x-section in a direct way and to compare the experimentally found values to the theoretical ones.

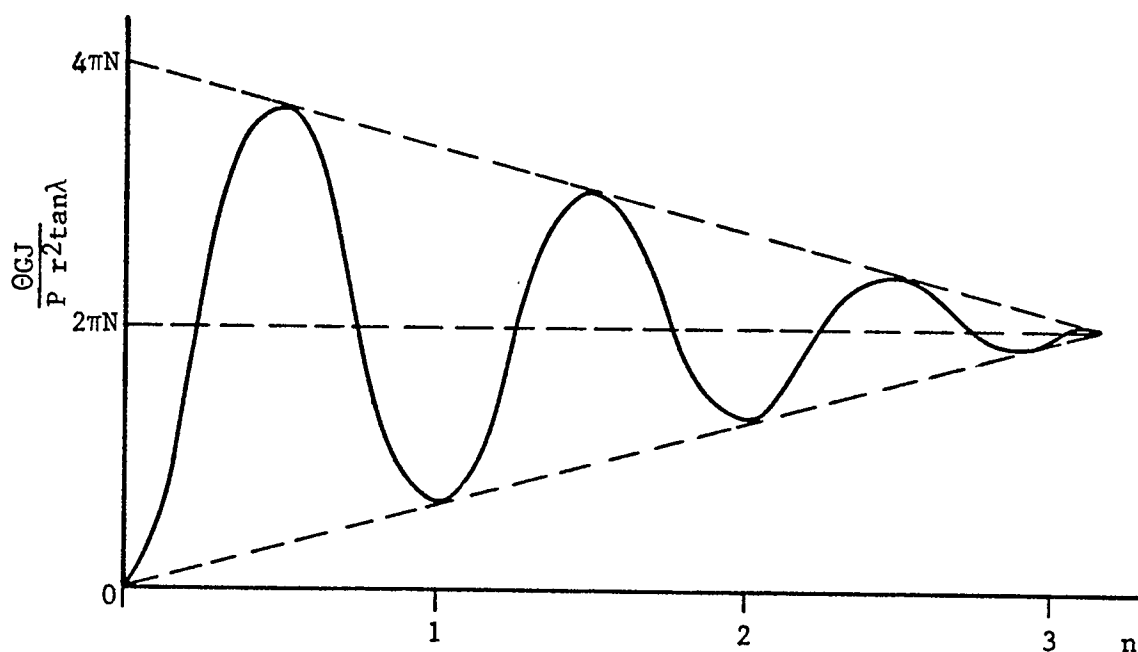


Figure (2.7) Rotation Angle of Free Coils Along the Helix.

Such a device (Figure 3.7) could also be used in later stages of the research to measure the actual values of rotation under the influence of friction forces.

Measurements are done at a fixed location for each coil for five different loadings. Results are shown below in Table (1):

| | | 1.40N | 2.40N | 6.32N | 12.76N | 19.13N |
|---------|--------------|-------|-------|-------|--------|--------|
| 1. Coil | Theoretical | 0.26 | 0.45 | 1.20 | 2.40 | 3.55 |
| | Experimental | 0.10 | 0.40 | 1.00 | 2.00 | 3.00 |
| 2. Coil | Theoretical | 0.25 | 0.43 | 1.10 | 2.30 | 3.41 |
| | Experimental | 0.10 | 0.40 | 1.00 | 2.10 | 3.10 |
| 3. Coil | Theoretical | 0.20 | 0.30 | 0.80 | 1.70 | 2.60 |
| | Experimental | 0.20 | 0.30 | 0.90 | 1.80 | 2.60 |
| 4. Coil | Theoretical | 0.10 | 0.20 | 0.50 | 1.10 | 1.76 |
| | Experimental | 0.00 | 0.10 | 0.40 | 0.90 | 1.30 |
| 5. Coil | Theoretical | 0.00 | 1.10 | 0.30 | 0.60 | 0.90 |
| | Experimental | 0.00 | 0.00 | 0.20 | 0.40 | 0.60 |
| 6. Coil | Theoretical | 0.00 | 0.00 | 0.00 | 0.00 | 0.10 |
| | Experimental | 0.00 | 0.00 | 0.00 | 0.00 | 0.00 |

Table (I) Comparison of Theoretical and Experimental Values of Relative Rotation of Coils in a Spring (microradians).

2.7. CONCLUSION

A simple model consisting of a helical spring wound around a cylindrical core is considered in order to analyze the principal mode of friction in the cables. The expression for the deflected center line of a helical spring subjected to transverse point load is derived and it is proved that the equivalent stiffness of a spring in shear is equal to that found by Timoshenko [30] in bending. This is the first time such a result has been presented.

Theoretically the equation derived for the lateral deflection of a spring is compared and found to be in very good agreement with the experimental results.

Then by comparing the expressions for the deflected center lines of a helical spring and a beam it is shown that the lateral slippage of coils inside a cable can be neglected and the rotation of coils is the primary mechanism of slippage and friction losses, Vinogradov and Atatekin [29].

In the second part, a Rotation Measuring Device (RMD) is developed, manufactured and used to measure the amount of rotation, occurring at different cross-sections of a helical coil subjected to a transverse point load.

Experimentally measured values of rotation are found to be in good agreement with the theoretical ones.

CHAPTER THREE

HYSTERESIS LOOP AT A CROSS-SECTION

3.1. INTRODUCTION

By taking a closer look at the expression for torque at any cross-section (equation 2.33), and the rotation angle for a free helical spring (Figure 2.7) it can be seen that the expressions for loading and deformation have periodic characteristics with varying magnitudes in each period. By also considering the simple physical model of a helical spring wound around a cylindrical core developed in Chapter One, it is easy to see that that simple model can be further simplified by isolating a small part of it from the rest of the model. Assuming the location and size of such "small parts" or "sections" can be found, then the internal losses in a cable can be explained in terms of the simplest model shown in Figure (3.1), Vinogradov and Atatekin [28].

Furthermore, since the forces acting are perpendicular to the center line of the helical coil, the physical model of Figure (3.1), can be shown to be mathematically equivalent to the model in Figure (3.2).

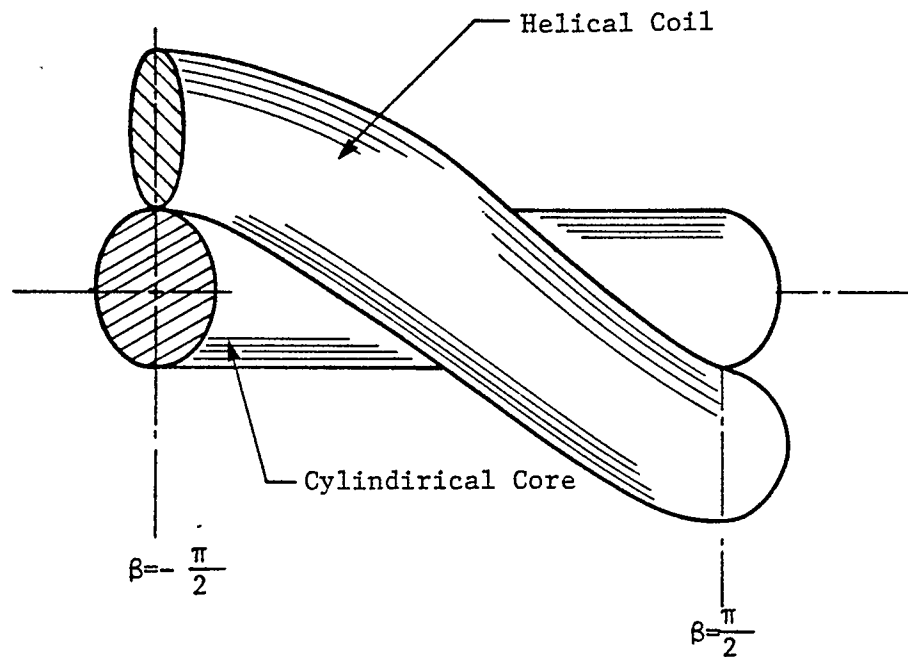


Figure (3.1) Basic Physical Model.

Uniformly distributed friction torque per unit length is assumed to exist between the coil and the core but if the coil doesn't rotate, friction torque is assumed to be zero. If the expressions for rotation angle versus applied internal torque can be derived for any cross-section within the small region model considered above, then the total loss for the whole cable can be found by simply summing up all such losses in each particular region along the cable axis, Vincigradov and Atatekin [28], [29].

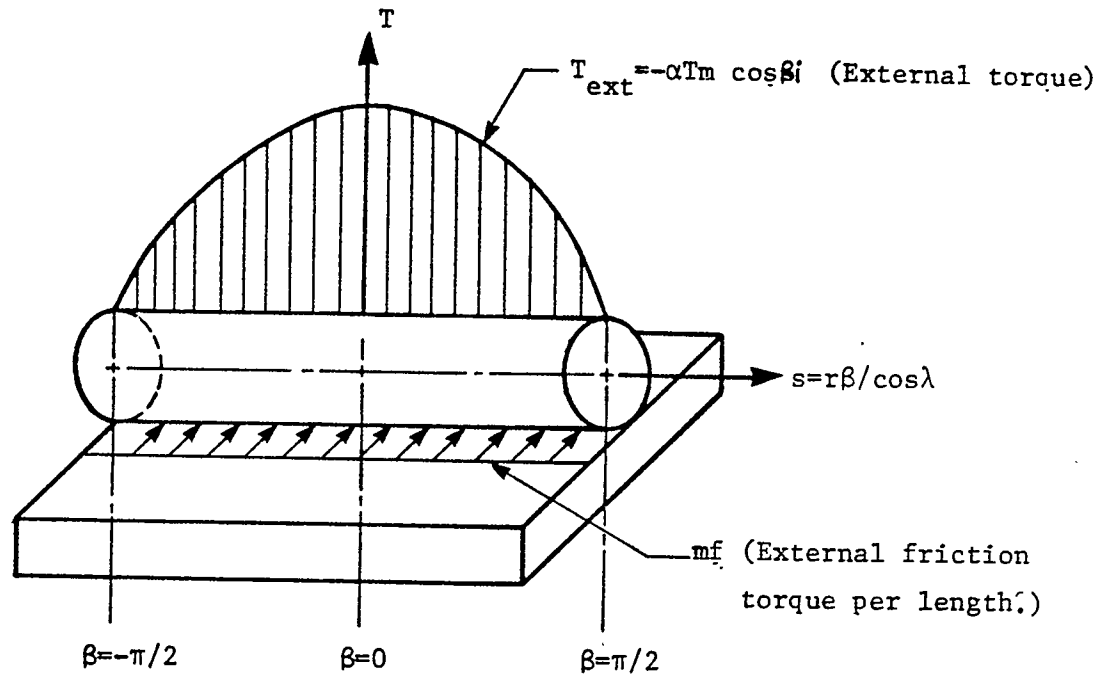


Figure (3.2) Mathematically Equivalent Model to
the Basic Element in Figure (3.1).

Assuming the same deflected centerline, the internal torque at any cross-section is the same for a "free" spring and for a spring with friction force acting on it. It should be emphasized here that there is no doubt that a spring with friction will deflect less under the same load compared to that of a "free" spring. However, as long as the general shape of the deflected center line remains similar, internal torque resulting from applied load can be assumed to be the same even though the "net" internal torque changes dramatically.

3.2. TWISTING MODE OF COIL DEFORMATION

Recalling the expression for twisting torque caused by a concentrated load (equation 2.33) at any cross-section of a helical coil:

$$M_t = -Pr \sin\lambda [\cos\phi + (2\pi N - \phi) \sin\phi] \quad (3.1)$$

By neglecting the asymmetry of the torque distribution within one coil turn, equation (3.1) can be simplified as:

$$M_t = -\alpha P_m r \sin\lambda [\cos\phi + 2\pi(N - n) \sin\phi] \quad (3.2)$$

where

P_m = maximum magnitude of the load

α = variable coefficient $-1 \leq \alpha \leq 1$

In order to find the location of small sections where slippage occurs, or in other words, to find the location of points for which external torque is maximum, internal torque (equation 3.2) is equated to zero and solved.

$$\alpha P_m r \sin\lambda [\cos\phi + 2\pi(N - n) \sin\phi] = 0 \quad (3.3)$$

$$\phi_m = \tan^{-1} \left[- \frac{1}{2 \pi(N - n)} \right] \quad (3.4)$$

which gives the locations of middle points of all the slipping sections for $n = 0.5, 1, 1.5, \dots, N$.

By introducing a new variable:

$$\beta = \phi_m - \phi \quad (3.5)$$

equation (3.2) can be expressed as:

$$T = \alpha T_m \sin \beta \quad (3.6.a)$$

where

$$T_m = P_m r \sin \lambda [\sin \phi_m - 2\pi(N - n) \cos \phi_m] \quad (3.6.b)$$

It is important to keep in mind that the equation (3.6) is the expression for internal torque at any cross-section of the helical coil due to the applied load at the free end. The corresponding external torque that would result in the same internal torque can be found as:

$$T_{ext} = -\alpha T_m \cos \beta \quad (3.7)$$

Since it has been proved before that the deflected centerlines for a beam and a helical coil are **similar**, an external loading of the kind expressed in equation (3.7) can be assumed to be acting on any cross-section of the coil as a result of the deflected centerline.

Here it should be noted that the general form of equation (3.6) is the same for any rotating section, except for the magnitude of T_m which is dependent on ϕ_m . Therefore an analysis of half of a section can be applied to all the rotating sections later by considering symmetry and changing the magnitude of T_m . For the rest of this chapter, a section as shown in Figure (3.2) will be analyzed and the load versus rotation curve will be derived for any cross-section within the rotating section boundary. In this analysis, loading will be varied in two stages; in the first stage load increases from zero to maximum ($0 \leq \alpha \leq 1$), and in the second stage from maximum to negative minimum ($1 \geq \alpha \geq -1$). A possible third stage is merely a repetition of second stage in the reverse order and does not require a separate analysis.

3.2.1. STAGE ONE ($0 \leq \alpha \leq 1$)

If the slippage of strands is possible, then different strands may slip simultaneously and interact with each

other. In accordance with the assumption made that contact stresses and coefficient of friction remain constant, these effects can be neglected as far as the resistance of the coil to the twisting is concerned. The slippage starts if a twisting torque overcomes the frictional forces within some length of the coil section being analyzed (see Figure 3.4). This length in terms of boundaries (β_{11}, β_{12}) can be found from the requirement of section equilibrium:

$$T(\beta_{11}) + T(\beta_{12}) - m_f S = 0 \quad (3.8)$$

where

$$S = r(\beta_{11} - \beta_{12}) / \cos\lambda \quad (3.9)$$

It follows from the symmetry of loading and geometry that $\beta_{11} = -\beta_{12} = \beta_1$, equation (3.8) can be written as;

$$\alpha T_m \cos\lambda \sin\beta_1 - m_f r \beta_1 = 0 \quad (3.10)$$

or

$$\Omega \sin\beta_1 - \beta_1 = 0 \quad (3.11.a)$$

$$0 \leq \Omega \leq \Omega_m \quad (3.11.b)$$

where

$$\Omega = \alpha T_m' / \gamma \quad (3.12)$$

" T_m' " and " γ " defined as

$$T_m = P_m r \sin \lambda T_m' \quad (3.13.a)$$

$$T_m' = \sin \phi_m - 2 (N - n) \cos \phi_m \quad (3.13.b)$$

$$\gamma = \frac{mf}{P_m \sin \lambda \cos \lambda} \quad (3.14.a)$$

$$\Omega = \alpha \left(\frac{P_m}{mf} \right) \frac{\sin 2\lambda}{2} [\sin \phi_m - 2\pi (N - n) \cos \phi_m] \quad (3.14.b)$$

From equation (3.14.b) it can be seen that the non-dimensional load factor " Ω " depends on the ratio of the applied load and the friction torque (P/mf) for a particular geometry of the cable and a fixed number of strands (N, n). It is the ratio (P/mf) rather than the individual forces that determines whether or not the coils will slip at any stage of loading. There is a limit, however, on the maximum value of the applied load (P_m) for a deflection within the linear limits. For $mf = 0$, coils

rotate for any value of P , as $\Omega = \infty$. If the value of mf is given and fixed then the non-dimensional load factor " Ω " changes from zero to Ω_{\max} , as the applied load changes from zero to P_{\max} .

For any given value of Ω , equation (3.11) defines the boundary of the slipping section " β ". Furthermore, it can be proved that a section starts slipping at $\beta = 0$ (Appendix II) when $\Omega = 1$ and continues to slip until $\beta_1 = \pi/2$ at $\Omega = \pi/2$ and after that point, any further increase in Ω does not cause an increase in β as it meets the rotation boundary of the next immediate section at $\beta = \pi/2$ which has the equal magnitude of torque acting on it in the reverse direction. Within the length of one coil turn there are two equal slipping sections, having opposite sense of twisting in accordance with the assumption of torque symmetry.

The angle of twisting (slippage) is found by the integration of the following differential equation:

$$GJ \frac{d^2 \theta_1}{d\beta^2} = - \frac{r}{\cos} \frac{dT}{d\beta} + \frac{mf r^2}{\cos^2 \lambda} \quad (3.15)$$

satisfying the boundary conditions:

$$\theta_1 = 0 \quad \text{at} \quad \beta = \beta_1 \quad \text{and} \quad \beta = \beta_{21} = -\beta_1 \quad (3.16)$$

the solution is:

$$\eta_1 = \Omega (\cos\beta - \cos\beta_1) + \frac{1}{2} (\beta^2 - \beta_1^2) \quad (3.17.a)$$

where

$$\eta_1 = GJ \theta_1 \cos^2\lambda / mf r^2 \quad (3.17.b)$$

and Ω as defined by equation (3.12). It can be shown that when:

$$1. \Omega = 1 \text{ (Section just starting to rotate, } \beta_1 = 0 \text{)} \quad (3.18.a)$$

$$\eta_1 = 0 \quad (3.18.b)$$

$$2. \Omega = \pi/2 \text{ (Rotation all across the section, } \beta_1 = \pi/2 \text{)} \quad (3.18.c)$$

$$\eta_1 = \frac{\pi}{2} \cos\beta + \frac{1}{2} (\beta^2 - \frac{\pi^2}{4}) \quad (3.18.d)$$

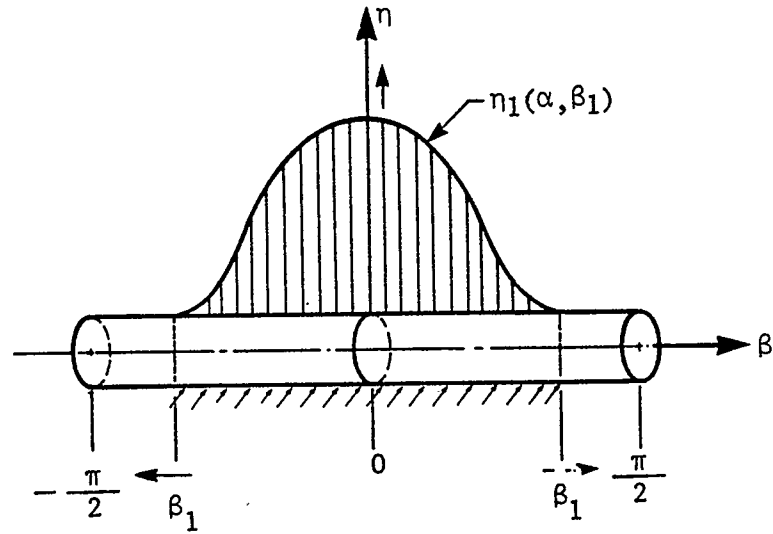


Figure (3.3) Slippage Along the Coil Section
During Stage One.

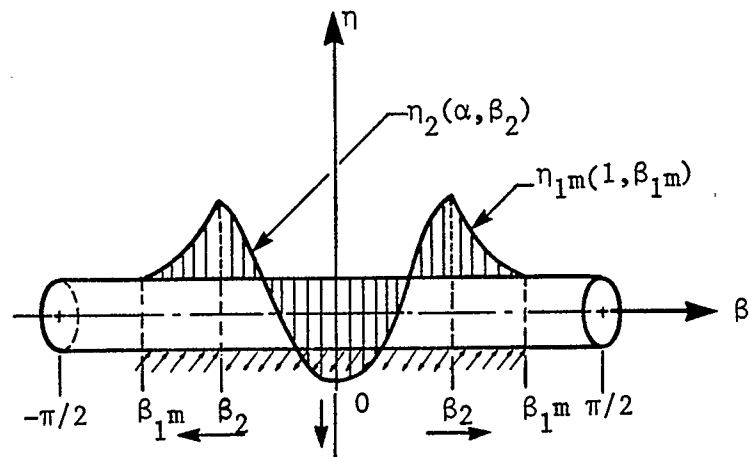


Figure (3.4) Slippage Along the Coil Section
During Stage Two.

and if

$$3. \quad \Omega \geq \pi/2 \quad (3.18.e)$$

$$\eta_1 = \Omega \cos\beta + \frac{1}{2} \left(\beta^2 - \frac{\pi^2}{4} \right) \quad (3.18.f)$$

where, to find the maximum slippage, $\beta = 0$ can be substituted into equation (3.18) which gives:

$$\eta_1 = \Omega - \frac{\pi^2}{8} \quad \text{for } \Omega \geq \pi/2 \quad (3.19)$$

At the end of the first stage $\alpha = 1$ and depending on the cable parameters $\Omega = \Omega_{\max}$ and $\beta_1 = \beta_{1\max}$ where $0 \leq \beta_1 \leq \pi/2$.

3.2.2. STAGE TWO ($1 \geq \alpha \geq -1$)

During this stage the external load decreases and the coil twists in an opposite sense. The boundary of a new slipping section $\beta_2 \leq \beta_{1\max}$ can be found from the requirement of equilibrium (see Figure 3.4). At the end of stage one, the torque acting in the cross-section $\beta = \beta_2$ is equal to

$$T_1(\beta_2) = T_m \sin\beta_2 - mf r \beta_2 / \cos\lambda \quad (3.20)$$

During the second stage, the decreasing load causes the following torque in the cross-section $\beta = \beta_2$:

$$T_2(\beta_2) = \alpha T_m \sin\beta_2 \quad (3.21)$$

Hence, the equation of section equilibrium, taking into account the external friction forces is:

$$T_1(\beta_2) - T_2(\beta_2) = mf r \beta_2 / \cos\lambda \quad (3.22)$$

Using equations (3.20), (3.21) and (3.22), the following equation defining the boundary β_2 is obtained:

$$(\Omega_m - \Omega) \sin\beta_2 - 2\beta_2 = 0 \quad (3.23)$$

where

$$\Omega_m = \Omega (\alpha=1) = T_m' / \gamma \quad (3.24)$$

By using a similar reasoning discussed in Appendix II, from equation (3.23) it can be found that the coil starts slipping in the opposite direction when $\Omega = \Omega_m - 2$ for which $\beta_2 = 0$. As Ω is decreased further down to

$\Omega = \Omega_m - \pi$, $\beta_2 = \pi/2$ and for $\Omega \leq \Omega_m - 2$, $\beta_2 = \pi/2$ again.
 If $\Omega = -\Omega_{max}$ is put into (3.23), the following equation can be obtained:

$$\Omega_m \sin \beta_2 - \beta_2 = 0 \quad (3.25)$$

which is similar to the equation (3.11) for $\Omega = \Omega_m$. By comparing these two equations, $\beta_{2max} = \beta_{1max} = \beta_{1m}$ is found. It means that the process is symmetrical.

The angle of twisting is described by differential equation (3.15) with the friction torque changing sign and the new boundary conditions:

$$GJ \frac{d^2 \theta_2}{d\beta^2} = - \frac{r}{\cos \lambda} \frac{dT}{d\beta} - \frac{mf r^2}{\cos^2 \lambda} \quad (3.26)$$

with

$$\theta_2 (\alpha, \beta_2) = \theta_1 (1, \beta_2) \quad (3.27.a)$$

$$\theta_2 (\alpha, -\beta_2) = \theta_1 (1, -\beta_2) \quad (3.27.b)$$

The solution is:

$$\eta_2 = \Omega (\cos\beta - \cos\beta_2) + \frac{1}{2} (2\beta_2^2 - \beta^2 - \beta_1 m^2) + \Omega m (\cos\beta_2 - \cos\beta_1 m) \quad (3.28)$$

It can be shown that when

1. $\Omega = \Omega_m$ (end of first stage)

$$\beta_2 = 0 \quad \eta_2 = \eta_{1\max} \quad (3.29.a, b)$$

2. $\Omega = \Omega_m - 2$ (coils are just starting to rotate in the reverse direction)

$$\beta_2 = 0 \quad \eta_2 = \eta_{1\max} \quad (3.29.c, d)$$

3. $\Omega = \Omega_m - \pi$

$$\begin{aligned} \beta_2 = \pi/2 \quad \eta_2 = (\Omega_m - \pi) \cos\beta + \frac{1}{2} \left(\frac{\pi^2}{2} - \beta^2 - \beta_1 m^2 \right) \\ - \Omega_m \cos\beta_1 m \quad (3.29.e, f) \end{aligned}$$

4. $\Omega = -\Omega_{\max}$

$$\beta_2 = \pi/2 \quad \eta_2 = -\eta_{1\max} \quad (3.29.g, h)$$

The third stage of loading ($-1 \leq \alpha \leq 1$) or $-\Omega_m \leq \Omega \leq \Omega_m$ is symmetrical to the second stage because

conditions of equilibrium remain the same. The difference is only in the direction of twisting.

3.3. HYSTERESIS LOOP AT A CROSS-SECTION

Derived expressions allow for any given magnitude of load, P (i.e. Ω) to determine the boundaries of slipping sections and the angles of slippage. For any cross-section of the coil this can be represented in the form of a hysteresis loop defining the work lost during one cycle of deformation.

By using equations (3.17) and (3.28) together with (3.18) and (3.29) the hysteresis loop shown in Figure (3.5) is obtained.

From Figure (3.5) it can be seen that the coil does not start rotating until $\Omega = 1.0$ in the first stage, and until $\Omega = \Omega_m - 2$ in the second stage. Distribution of rotation angle along the rotating section can be visualized as shown in Figure (3.3), and Figure (3.4).

3.4. COORDINATE TRANSFORMATION FOR SECOND STAGE

If the hysteresis loop at a cross-section (Figure 3.5) is carefully analyzed, it can be seen that the similar sections of the slippage curves for stages one and two are proportional to each other by a factor of two, e.g. $A'/A = B'/B = C'/C = 2$, therefore by using the following expressions:

$$\Omega = \Omega_m - 2\Omega^* \quad (3.30)$$

$$\eta_2 = \eta_m - 2\eta^* \quad (3.31)$$

The equations (3.28) and (3.23) can be put into the following forms:

$$\eta^* = \Omega^* (\cos\beta - \cos\beta_2) + \frac{1}{2} (\beta^2 - \beta_2^2) \quad (3.32)$$

with

$$\Omega^* \sin\beta_2 - \beta_2 = 0 \quad (3.33)$$

for which

$$0 \leq \Omega^* \leq \Omega_m$$

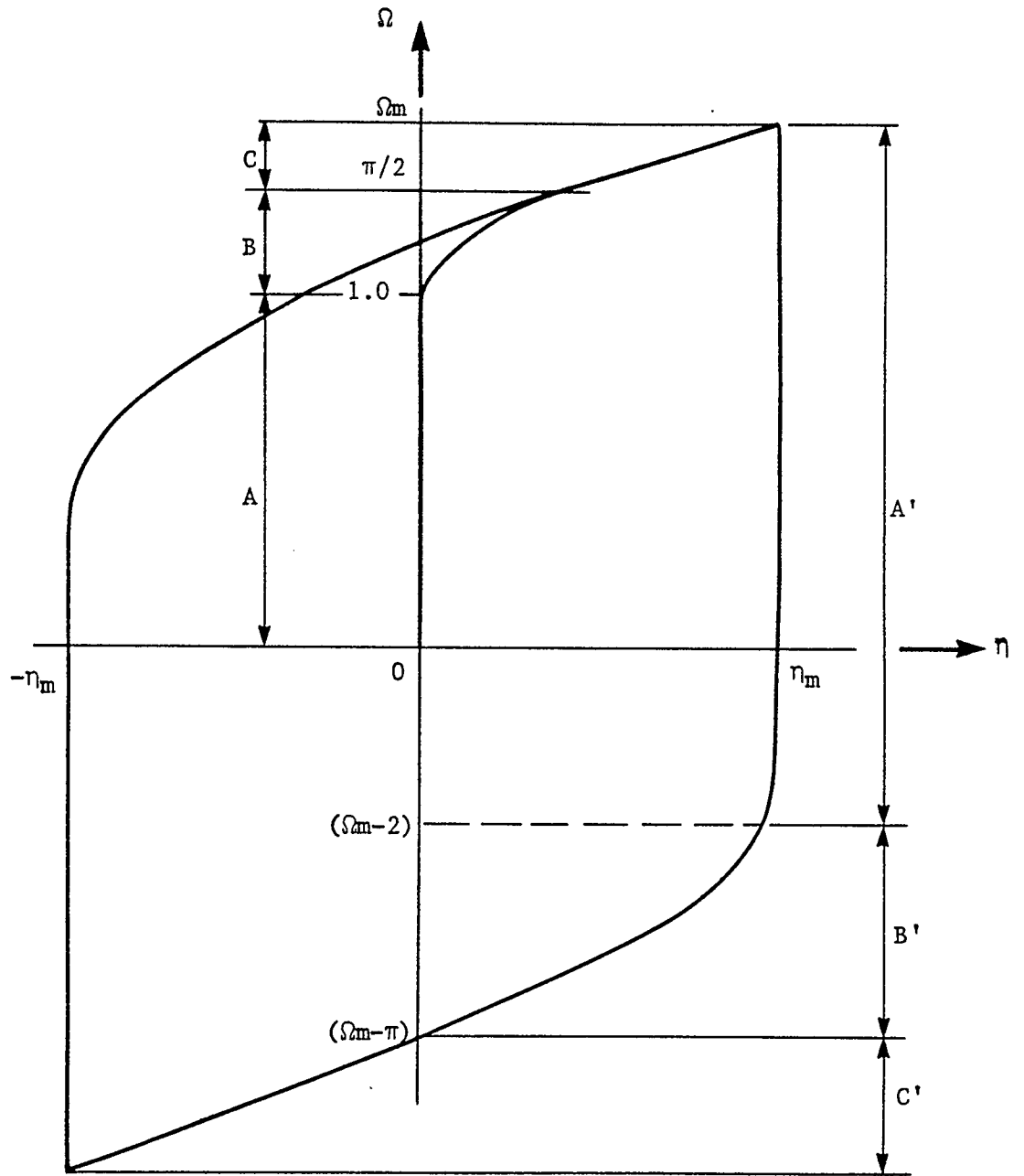


Figure (3.5) Hysteresis Loop at a Cross-section.

By comparing the equations (3.32) and (3.33) with (3.17.a) and (3.11), it can be seen that they are identical. It has been proved before that the equations for the third stage are identical to the ones for second stage with a change in signs of load and displacement. Now, the above transformation shows that there is actually one set of equations for boundary length and rotation at any stage of the hysteresis loop. By using the following transformations the amount of slippage and the boundary length for the second stage can be found from the expressions of the first stage:

$$\Omega_2 = \Omega_m - 2\Omega \quad (3.34)$$

$$\eta_2 = \eta_m - 2\eta_1 \quad (3.35)$$

for which

$$0 \leq \Omega \leq \Omega_m$$

3.5. EXPERIMENTAL RESULTS

After obtaining excellent results in measuring the rotation of helical coils of a "free" spring in Chapter Two, it was decided to try and see if the rotational slippage of coils of a spring on a cylindrical core can be

measured too. In order to be able to change the magnitude of friction force between the coil and the core, a set up as shown in Figure (3.6) was used.

Due to the length of time and cost involved in having a custom made spring with a precise internal diameter and lead angle, a stock auto shock spring was purchased. The middle part of the coil which had a reasonably constant lead angle ($9^{\circ} - 15^{\circ}$) was used for experiments. The internal diameter, however, was found to vary by a large amount from one point to another. In order to compensate for this, the thinnest available metal sheet that could also withstand the internal pressure without buckling was chosen. The pressure between the coil and the core, or the contact friction forces were controlled by means of a hydraulic pump connected to a bicycle inner tube.

In spite of the flexible thin metal plate used as an inner lining, a considerable number of non-touching surface sections of coil and core could be observed by the naked eye (Figure 3.7). Measurements were taken only at the sections that appeared to have a possible even contact at least for the distance between the clipped legs of the Rotation Measuring Device (RMD).

Also the RMD developed earlier for measuring the rotations of a "free" coil was found to be not sensitive enough for measuring rotations of a coil under friction

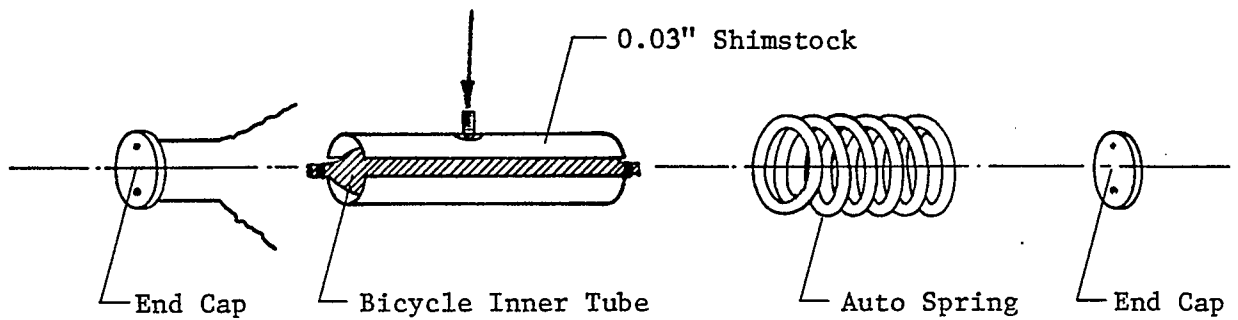


Figure (3.6) Experimental Set-up for Core Coil Model.

loading. A 20 times more sensitive RMD was designed and built by increasing the height of its legs and the length of the beam with strain gages.

Experimentally obtained hysteresis loops are shown in Figure (3.8). It should be noted that the loops shown are obtained by relative displacement of two cross-sections. It can be proved that the shape of a hysteresis loop obtained by relative displacement of two cross-sections will again be similar to the one shown in Figure (3.5). In all but one curve shown in Figure (3.8), the cross-sections start rotating slightly as soon as the direction of load is reversed. This can be attributed to the mechanical connection between the beam and the tips of the RMD. As

the sensitivity of the RMD was increased by a factor of 20, it has also become sensitive to the axial bending due to the friction between pointed ends and the beam.

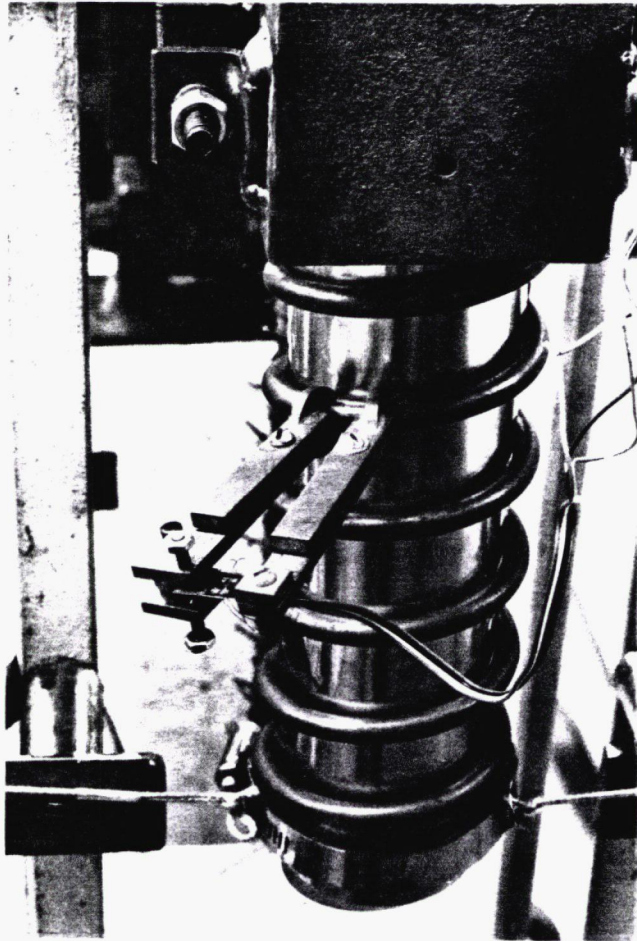


Figure (3.7) Experimental Set-up for Measurements.

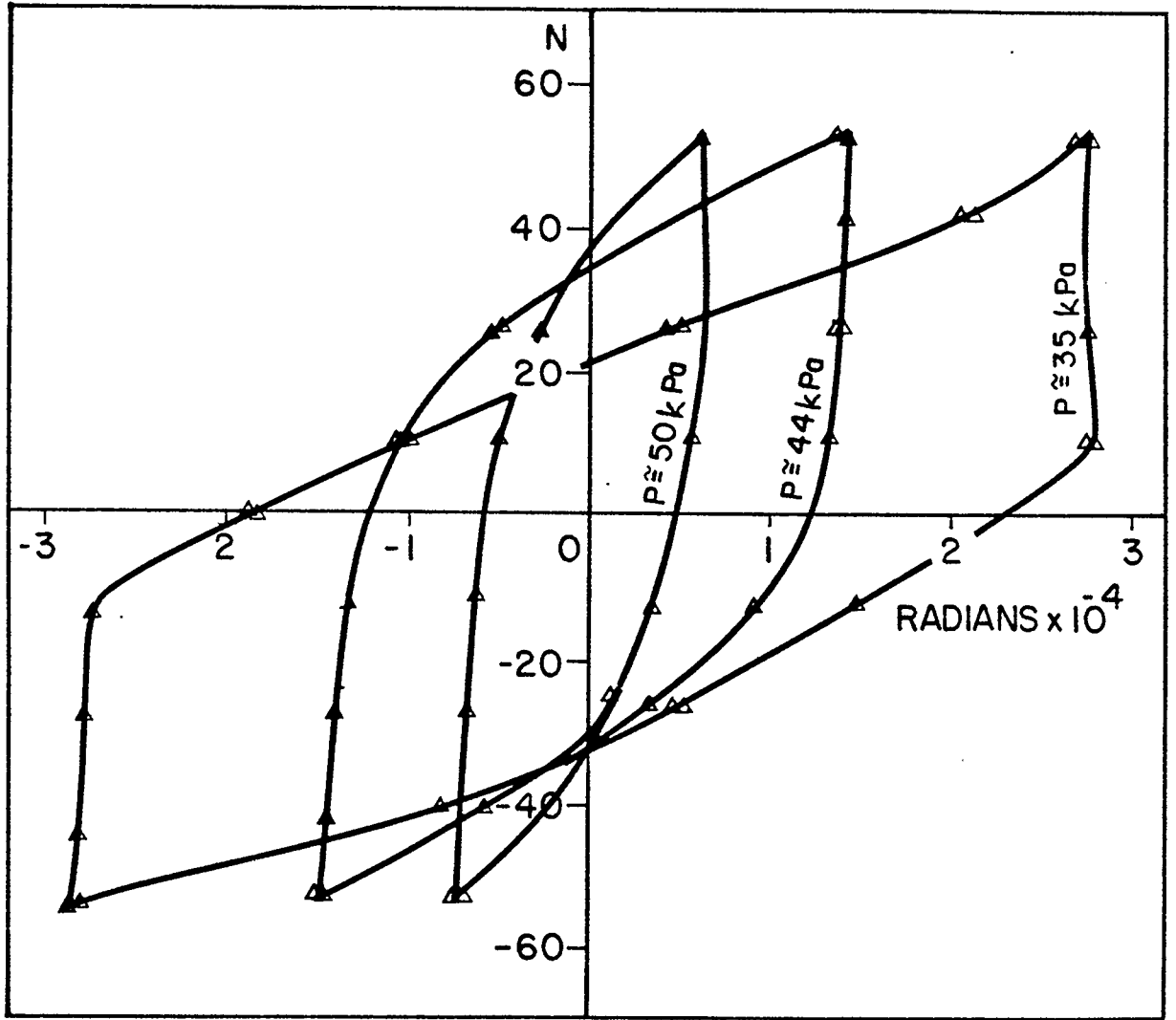


Figure (3.8) Hysteresis Loops Obtained from Experiments.

3.6. CONCLUSION

Due to periodic symmetry of loading and geometry of the helical coil wound around a cylindrical core, it is shown that the internal losses in a cable can be analyzed in terms of short sections that occur along the cable length. A theoretical model mathematically equivalent to the actual physical model is developed. Assuming Coulomb Friction, cable slippage and the propagation of a slippage boundary is investigated for two stages of loadings. It is shown that there is a minimum value of load after which the coil section starts slipping. By further noting the relationship between the slippage curves for initial and subsequent loading, it is demonstrated that the slippage curve for the second stage can be derived from the expressions for the first stage by means of transformation equations (3.34) and (3.35).

A second RMD 20 times more sensitive than the one used for measuring free rotation of coils, is designed and manufactured. Due to inconsistencies in the geometry of the spring being measured, only the hysteresis loops resulting from the relative slippages of the coils could be measured. Not having been able to obtain information on the real contact stresses and friction forces, only the

form of the experimentally obtained hysteresis loops could be compared with those of theoretical ones. Keeping in mind the shortcomings of the mechanical device used for measuring slippage, good qualitative agreement is obtained between theoretical and experimental results.

Before closing, it is important to emphasize the universality of the hysteresis loop shown in Figure (3.5). Since it is at a cross-section of a coil section and expressed in non-dimensionless quantities, the loop shown in Figure (1.1) represents the hysteresis at any cross-section of any cable with any geometrical parameters as long as the basic structure of the cable is composed of the one or several geometries shown in Figure (1.1).

CHAPTER FOUR

GENERAL FORMULATION FOR CABLE GEOMETRY

4.1 INTRODUCTION

The existence of the relationship between interstrand slippage and the change of stiffness of cables has long been recognized in the literature. It is stated by Claren and Diana [7] that the experimental tests performed previously have shown that the average stiffness of a vibrating cable has generally half the value which is obtained from calculations made with the assumption that the individual wires will not slip and the entire cross-section of the cable will act as a unit. Calculations made with the assumption that each wire acts individually would give stiffness values corresponding to 1.5-2.0 percent of those obtained with no individual wire slippage, that is, of a homogenous beam. It was then thought to be preferable by Claren and Diana [7] to analyze the dynamic strain distribution on taut homogenous beams and then investigate experimentally how a real stranded cable will differ from the theoretical model and make corrections by introducing slippage coefficients.

In other papers by Wagner and others [6], [20], [19], [21], the experimentally obtained load-deflection curve for a cable is considered and it is stated that the experimental bending stiffness of a cable is considerably less than that obtained by taking the product of Young's Modulus of cable material and the second moment of area of cross-section about its neutral axis. The difference is attributed to the slip between the strands of the cable.

In this chapter it is proven that the change in the stiffness of the cable can be explained in terms of the slipping sections of finite length. After deriving the expressions for slippage at any cross-section of a slipping section, the next step in understanding the internal slippage of cables is to construct a full scale model built of small sections described in Chapter Three. As was stated earlier, the slippage section is a common property of cables and can be found in cables of any geometry and any number of strands. Formulation of a full scale model, however, by combining such slippage sections, proves to be difficult due to the complex geometry of cables with a large number of strands.

As the simplest geometry used in real life, the cable shown in Figure (1.1) will be used to analyze internal slippage. Solutions for cables of more complex geometries composed of several combinations of the cable shown in

Figure (1.1) can be derived by using a somewhat similar procedure.

4.2 GENERAL FORMULATION FOR CABLE GEOMETRY

The assumption of aligning the x-axis with the central axis of the helical coil was made in Chapter Two to simplify the resulting equations without any loss in the application to general cases. If five more additional coils are added to the helical coil and core model of Figure (2.1) to obtain the basic cable structure shown in Figure (1.1), the following terminology and numbering system is introduced to clearly define any cross-section at any point of the cable.

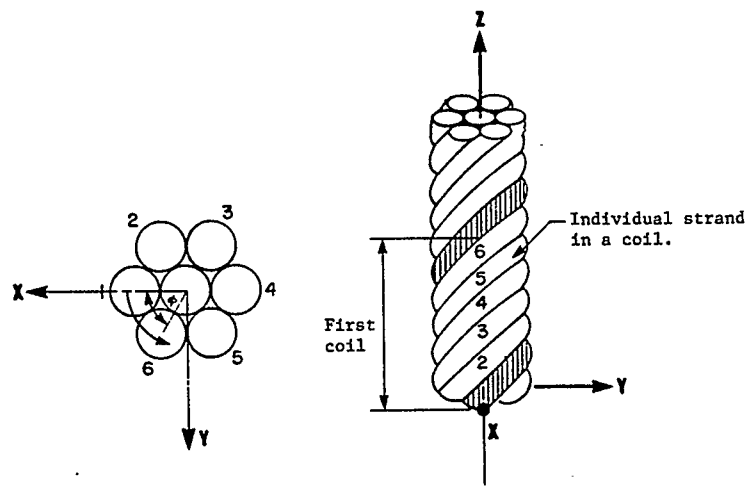


Figure (4.1) Numbering of Strands and Location of Reference Axes in a Cable.

As seen in Figure (4.1), the first strand in the first coil starts at $\phi = 0^0$. A clockwise direction is chosen for numbering the strands. Positive direction of central angle is counter-clockwise. Strands are referred to by their strand number and coil number (e.g. Third strand in second coil etc.).

The equation defining any strand in a cable with number of strands (in our case $K = 6$) can be written as follows:

$$x_i = r \cos\phi \quad y_i = r \sin\phi \quad z = k' \left[\phi + (i-1) \frac{2\pi}{K} \right] k \quad (4.1)$$

for $i=1,2,3,\dots,K$

where $k' = \frac{h}{2\pi n}$ as before

and starting points on $z = 0$ plane can be found from:

$$\phi_{0i} = - (i - 1) \frac{2\pi}{K} \quad i = 1,2,\dots,K \quad (4.2)$$

By taking $K = 6$ in equations (4.1) and (4.2) and using a procedure similar to the one used in Section (2.2), the torsional moment acting at any cross-section of any strand can be found from:

$$M_{ti} = -P_m r \sin\lambda \left\{ \cos\phi_i + \left[2\pi(N-n) - (i-1) \frac{\pi}{3} \right] \sin\phi_i \right\} \quad (4.3)$$

Location of the center of the slipping sections can be found by:

$$M_{ti} = 0 \quad (4.4)$$

which gives:

$$\phi_{mi} = \tan^{-1} \left[- \frac{1}{2(N-n) - (i-1) \frac{\pi}{3}} \right] \quad (4.5)$$

with:

$$T_i = \alpha T_{mi} \sin\beta \quad (4.6)$$

where

$$T_{mi} = P_m r \sin\lambda T_{m'i} \quad (4.7.a)$$

$$T_{m'i} = \sin\phi_{mi} - \left[2\pi(N-n) - (i-1) \frac{\pi}{3} \right] \cos\phi_{mi} \quad (4.7.b)$$

where

number of coils $n = 1, 2, \dots, N$

i = number of strands in each coil, e.g.
 $i = 1, 2, \dots, 6.$

4.3 BOUNDARY OF THE SLIPPING SECTIONS

As mentioned before, the form of the loading function on the slipping section (equation 4.6) does not change with respect to its location. Only the magnitude of the constant (T_{mi}) changes from one strand to another. Therefore the expressions derived for the boundary and the amount of slippage (equations 3.11 and 3.17.a) can be used by replacing " T_m " in those equations by " $T_m'i$ ".

The expression that gives the boundary for a slipping section is:

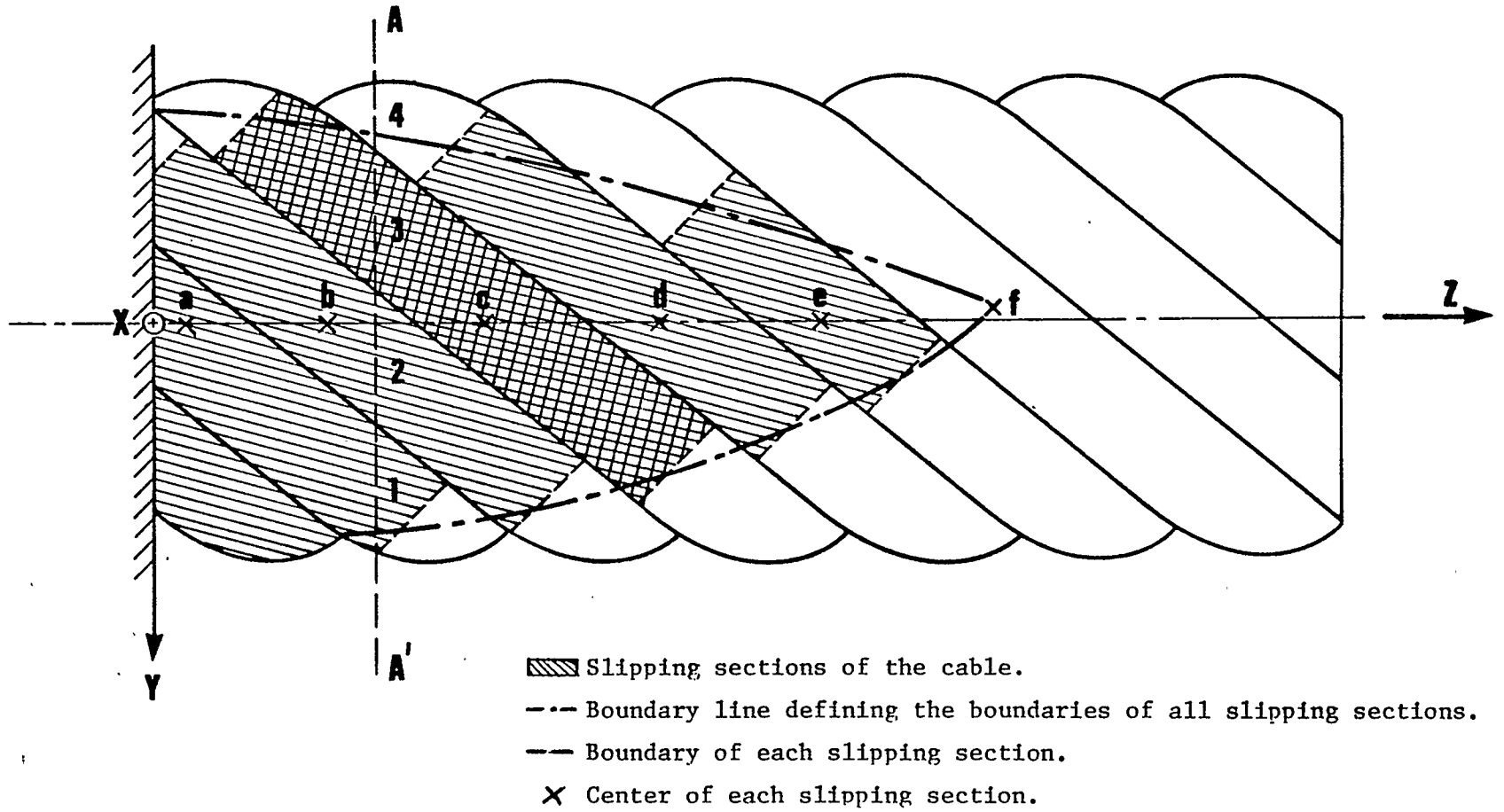
$$\Omega_i \sin \beta_{1i} - \beta_{1i} = 0 \quad (4.8)$$

where

$$\Omega_i = \alpha T_m'i / \gamma \quad (4.9)$$

$$\gamma = \frac{mf}{P_m \sin \lambda \cos \lambda} \quad (4.10)$$

Figure (4.2) Boundary of the Slipping Sections.



At any stage of loading, the collection of points defined by ϕ_{mi} and β_{1i} describes the boundary of the end points of rotating sections. To better visualize such a "boundary of boundaries" a rather schematic two-dimensional projection of the cable onto the y-z plane is shown in Figure (4.2).

To better understand the picture shown in Figure (4.2), it should be noted that the dark shaded area shown can be taken as the top view of the coil shown in Figures (3.4) and (3.5). As the applied load at the end of the cable reaches a critical value, the first coil starts to slip at "a" and as the load continues to increase the boundary of slippage propagates in the direction of the arrows shown and new centers of slippage continue to form (e.g. b, c, d, ...etc.)

At a typical cable cross-section AA' as shown in Figure (4.2), cross-sections of the the strands 1, 2, and 3 slip, as they are within the boundary line defining the boundaries of all slipping sections.

Section AA' is also shown on the x-y plane in Figure (4.3). It can be seen from Figure (4.3), that the contribution of those three slipping sections to the total moment of inertia of the cable is only $3 I_w$. In the case of no slippage, however, contribution from those three sections rises to $[3I_w + 3\pi R^2 (r^2 \sin^2 \phi_1 + r^2 \sin^2 \phi_2 + r^2 \sin^2 \phi_3)]$.

Change in the moment of inertia of the cable due to slipping strands of each cross-section is found first by using a numerical method and then by a simplified method in the next section.

A close examination of Figure (4.2) reveals that the locations of uniform levels of strains do not exist either along a specific strand or on two adjoining strands. This finding is supported by the experiments done by Claren and Diana [7] who report that even with the same static load on wires, considerable differences can still be found on strain values measured on two different, but closely associated wires. It is therefore stated that [7] no strain measurements made on a single wire can be taken as representative of the strain level of that particular cross-section of the cable.

The distance between the boundary of the slipping sections and the y and z-axes can be written as follows:

$$y(i)/r = \sin (\phi mi + \beta_1 i) \quad (4.11)$$

$$z(i)/h = [2\pi n + (i-1) \frac{\pi}{3} + \phi mi + \beta_1 i] / 2\pi N \quad (4.12)$$

Since it is also known that all the cables loosen only for part of the total length (i.e. $n \ll N$), by examining

equation (4.5) it can be proven that $\phi_{mi} \approx 0$ for the slipping part of the cable which is in most cases less than 30 % of the total length. Also for the same reason, the boundary of the slipping section is taken to be symmetrical with respect to the z-axis, in spite of the fact that some asymmetry will occur due to the helix angle " λ ".

4.4 CHANGE IN MOMENT OF INERTIA

For easier derivation, a reverse process is developed to express the change in the moment of inertia in terms of the boundary of the slipping sections. Instead of taking "any" cross-section and determining whether or not each strand rotates in that cross-section, first a specific strand is chosen, the boundary of rotation for that strand is found from equation (4.12) and then the cross-section of the cable at the slippage boundary of that particular strand is analyzed. Then a simple test is needed to determine whether the rest of the strands at that cross-section rotate or not.

A lengthy TI-59 programme was written following a procedure explained below. For the ease of calculations the term "n" is omitted in the following equations and instead "i" is used as $i = 1, 2, \dots, 6$ N.

4.5 ALGORITHM

1. For each strand, the boundary of slippage is found from equation (4.8):

$$\Omega_i \sin \beta_{1i} - \beta_{1i} = 0 \quad i = 1, 2, \dots, 6N \quad (4.13)$$

2. β_{1i} found from the above equation is **substituted into** equation (4.12) to determine the cross-section that will be analyzed:

$$z(i)/h = [2\pi n + (i-1) \frac{\pi}{3} + \beta_{1i}] / 2\pi N \quad (4.14)$$

3. Orientation of the reference strand (which has $\phi = 0$ at $z = 0$) is found from:

$$\phi_1 = \beta_{1i} + (i-1) \frac{\pi}{3} \quad (4.15)$$

4. Orientation of the other strands (at the cross-section found in step 2) can be found as:

$$\phi_j = \phi_1 - (j-1) \frac{\pi}{3} \quad j = 1, 2, \dots, 6 \quad (4.16)$$

5. The orientation of the strand cross-section that constitutes the boundary for the slipping strand cross-sections at the cross-section of the cable found in step 2:

$$\phi_i = \phi_{mi} + \beta_i \quad (4.17)$$

but $\phi_{mi} = 0$, therefore $\phi_i = \beta_{1i}$ (4.18)

6. Whether or not the rest of the strands slip can be determined by the following test (see Figure 4.3):

$$\text{If } |\sin\phi_j| \leq |\sin\beta_{1i}| \text{ then } \sin\phi_j = 0 \quad j = 1 \dots 6 \quad (4.19)$$

For example, in Figure (4.3), $i = 1$ and the cross-section at $\phi_1 = \beta_{11}$ is considered. Since it is also known that the center of the slipping section is located on $y = 0$, any strand cross-section with a center between ϕ_1 and the $y = 0$ line must be slipping. By considering the symmetry of the slipping sections around the $y = 0$ axis, it can be seen that strands 1, 2 and 3 are slipping in Figure (4.3). By further considering the opposite side of the coil with a reverse sign of torque and angle of slippage, it can be concluded that if strand 1 slips at the cross-section shown, then all the strands slip. However if

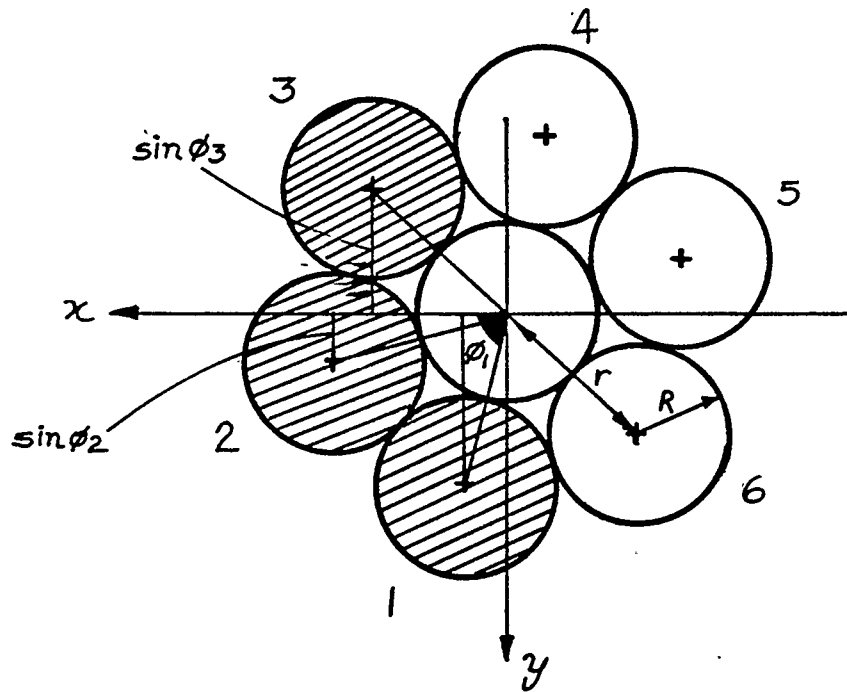


Figure (4.3) Slippage of Strands at a Cross-section.

3 was the critically slipping strand, then only strands 3, 2, 5 and 6 would be slipping. Equation (4.19) automatically provides the number of strands that slip at any cross-section.

7. Moment of Inertia at any cross-section of the cable can be found from:

$$I = \frac{\pi R^4}{4} + \sum_{j=1}^6 \left[\frac{\pi R^4}{4} + \pi R^2 (r \sin \phi_j)^2 \right] \quad (4.20)$$

which can be simplified for $r = 2R$ and $I_w = \pi R^4/4$:

$$I/I_w = 7 + 16 \sum_{j=1}^6 \sin^2 \phi_j \quad (4.21)$$

It should be noted that in all of the above equations, cross-sections of strands on the x-y plane are assumed to be perfect circles. Due to the helix angle " λ ", however, cross-sections are slightly elliptical and a more exact expression could be written as follows:

$$I/I_w = (1 + 6 \sin^2 \lambda) + 16 \sin^2 \lambda \sum_{j=1}^6 \sin^2 \phi_j \quad (4.22)$$

For most practical applications, $\lambda \geq 80^\circ$, the error introduced is less than 2 % by using the equation (4.21).

A diagram obtained by using the above explained algorithm is shown in Figure (4.4). It should be noted that owing to the use of load coefficient " Ω ", Figure (4.4) represents the change in the "I" of a cable with a structure as shown in Figure (1.1) and of any physical dimension. It can be that $I/I_w = 55$ for a non-slipping cross-section, and $I/I_w = 7$ for a completely loose cross-section, which represents an 87 % reduction in rigidity of the cable.

Although the algorithm explained above is exact and explains the strand slippage in detail, it is not in a **useful form for a use in later stages of formulation.** Therefore, an alternative approach will be sought to express the change in I in terms of simple expressions.

It is proven in Chapter 2 that when $\Omega = 1$, slippage starts and when $\Omega = \pi/2$, the section slips all the way up to $\beta = \pi/2$, to meet the boundary of slippage in the opposite direction at the other half of the coil.

By introducing " Ω_0 " which is the value of Ω at the first strand of the first coil for any applied load at the end of the cable, Ω_i for any strand can be written as follows:

$$\Omega_i = \frac{\Omega_0}{2\pi N} T_m' i \quad (4.23)$$

By taking $\phi_{mi} \approx 0$ at the equation (4.7.b) and using only one counter for strands (i.e. i) instead of both " n " and " i " so that now $i = 1, 2, \dots, 6N$:

$$T_m' = 2\pi N - (i - 1) \frac{\pi}{3} \quad (4.24)$$

To find the specific strand with a $\Omega i = 1$, equations (4.13) and (4.14) can be combined to determine the critical strand number:

$$i_A = 6N \left(1 - \frac{1}{\Omega_0} \right) + 1 \quad (4.25)$$

It can be reasoned that any strand with a strand number greater than i_A does not contain any slipping sections, or in other words, there is no internal slippage of the cable after the i_A th strand. It should be kept in mind that as $\phi m i \approx 0$, $\phi m i$ centers for all the strands are on the x-z plane. Therefore, by defining the i 'th strand, the intersection of i_A 'th strand with x-z plane can be taken to define the beginning of the non-slip section in the cable. Therefore equation (4.15) can be used to find the length of the non-slipping part of the cable as a percentage of the total length:

$$A = \frac{i_A}{6N} = 1 - \frac{1}{\Omega_0} + \frac{1}{6N} \quad (4.26)$$

A = Percent distance from the fixed end of the cable at which slippage in the cable ceases to exist.

By using the same reasoning for $\Omega i = \pi/2$, the critical strand number before which all the strands at any cross-section slip can be found as:

$$i_B \approx 6N \left(1 - \frac{\pi}{2\Omega_0} \right) + 1 \quad (4.27)$$

or in terms of percent distance:

$$B = \frac{i_B}{6N} = 1 - \frac{\pi}{2\Omega_0} + \frac{1}{6N} \quad (4.28)$$

B = Percent distance from the fixed end of the cable at which total slippage at the cross-section ceases to exist. The distance from B to A is a transition region. At any cross-section between B and A , only some of the strand cross-sections slip. It can be seen from Figure (4.4) that the transition in the BA region is in terms of rather large jumps in a non-linear fashion. Since the length of the transition region is rather small (10 % max.) compared to the total length of the cable, the change in "I" will be assumed to be linear.

When equations (4.26) and (4.28) are compared with the results obtained from the algorithm mentioned before for different values of Ω_0 , excellent agreement is found

between equation (4.26) and the algorithm. However, the $\pi/2$ term in equation (4.28) had to be replaced empirically by 1.22 as the curvature of the coils at $\beta = \pi/2$ causes very little increase in the I as β just starts to decrease from $\pi/2$. By also neglecting the term $1/6 N$ compared to the other terms (2 % error for $N = 6$), equations (4.26) and (4.28) can be rewritten as follows:

$$B = 1 - \frac{1.22}{\Omega_0} \quad (4.29)$$

$$A = 1 - \frac{1}{\Omega_0} \quad (4.30)$$

Therefore, the following expressions can be written for different levels of loading (Ω_0):

$$1. \quad \Omega_0 \leq 1$$

No slippage at any cross-section of the cable:

$$I / I_w = 55 \quad \text{for } 0 \leq z \leq h \quad (4.31)$$

$$2. \quad 1 \leq \Omega_0 \leq 1.22$$

Clamped end of the cable starts to slip partially. (No complete slippage) Assuming linear change in "I":

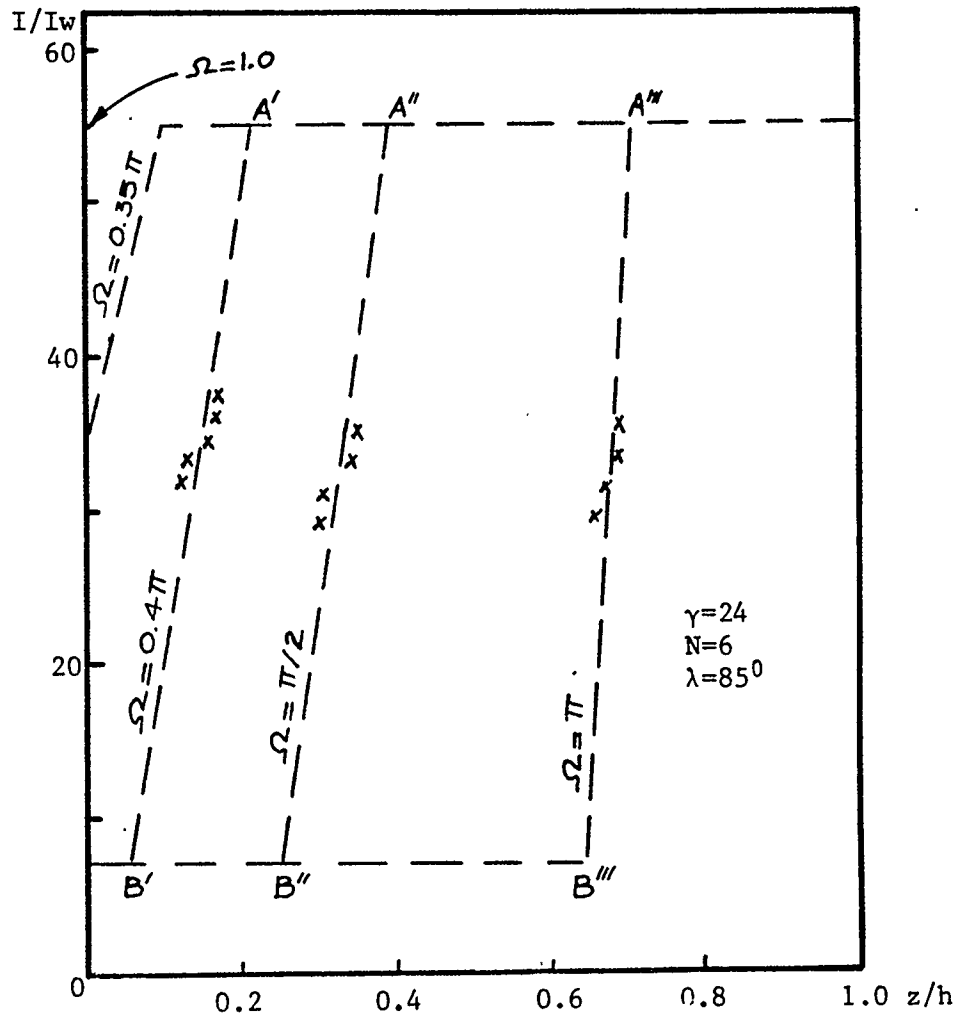


Figure 4.4 Change in the Stiffness of a Cable

$$I/I_w = 55 - 48(z-A)/(B-A) \quad 0 \leq z \leq Ah \quad (4.32.a)$$

$$I/I_w = 55 \quad Ah \leq z \leq h \quad (4.32.b)$$

3. $1.22 \leq \Omega_0$

All three (complete slip, partial slip, complete non-slip) regions are present in the cable):

$$I/I_w = 7 \quad 0 \leq z \leq Bh \quad (4.33.a)$$

$$I/I_w = 55 - 48(z-A)/(B-A) \quad Bh \leq z \leq Ah \quad (4.33.b)$$

$$I/I_w = 55 \quad Ah \leq z \leq h \quad (4.33.c)$$

4.6 BENDING ENERGY STORED IN THE CABLE

The expression for bending energy in the most general form for the cable shown in Figure (4.5) can be written as follows:

$$W_b = \frac{1}{2} \int_0^{x_1 h} \frac{P^2 x^2}{E I_N} dx + \int_{x_1 h}^{x_2 h} \frac{P^2 x^2}{E I(x)} dx + \int_{x_2 h}^h \frac{P^2 x^2}{E I_R} dx \quad (4.34)$$

where

$P = \alpha P_m$, load applied at the free end

$$I_N = 55 I_w$$

$$I_R = 7 I_w$$

$$I(x) = I_w \left[55 + \frac{48A'}{(B'-A')} - \frac{48x}{(B'-A')h} \right] \quad (4.35)$$

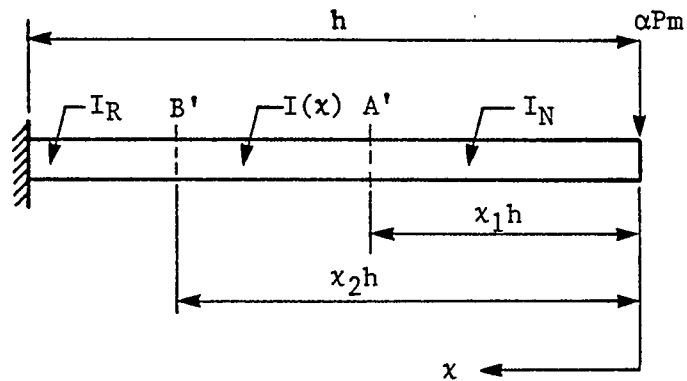


Figure (4.5) Bending Energy Stored in a Cable.

If equation (4.35), is substituted into equation (4.34) and integrated:

$$W_b = \frac{P^2 h^3}{2EI_w} \left[\frac{x_1^3}{165} + \frac{(1-x_2^3)}{21} - \frac{(x_2^2-x_1^2)}{2 C_2} - \frac{C_1}{C_2^2} (x_2-x_1) \right]$$

$$-\frac{C_1^2}{C_2^3} \ln \frac{(C_1 - C_2 x_2)}{(C_1 - C_2 x_1)} \quad (4.36)$$

with

$$C_1 = 273.18 \quad (4.37.a)$$

$$C_2 = 218.18 \Omega_0 \quad (4.37.b)$$

and if

$$1. \quad 0 \leq \Omega_0 \leq 1 \quad x_1 = x_2 = 1 \quad (4.38)$$

$$2. \quad 1 \leq \Omega_0 \leq 1.22 \quad x_1 = A' \quad x_2 = 1 \quad (4.39)$$

$$3. \quad 1.22 \leq \Omega_0 \quad x_1 = A' \quad x_2 = B' \quad (4.40)$$

where

$$A' = 1/\Omega_0 \quad (4.41)$$

$$B' = 1.22/\Omega_0 \quad (4.42)$$

or a programming trick used should be mentioned here:

$$x_1 = A' \quad x_2 = B' \quad \text{always}$$

but if $A'.GE.1$, $A' = 1$

if $B'.GE.1$, $B' = 1$

4.7 CONCLUSION

In this chapter it is shown that the cable internal slippage can be explained in terms of local slipping sections on each strand. The expressions derived in previous chapters are generalized to formulate any slipping at any cross-section of any strand. After defining each slipping section at their respective places, a macroscopic view is employed in an attempt to predict their behaviour as a whole. An expression for the boundary of the end points of all the slipping sections is derived and the concept is explained pictorially. It is shown that if a strand slips at any cross-section of the cable, it then bends along its own axis rather than the axis of the cable which results in considerable reduction in the stiffness of the cable. Later, the idea of the boundary of the slipping sections is taken one step further to determine the number of slipping strands at each cross-section to develop an algorithm for finding the "I".

The algorithm developed however, proves to be clumsy for developing an expression for bending energy to be used in later chapters. By using another approach explained in Section 4.4.1, very useful formulas are developed for

expressing the boundaries of complete slippage, partial slippage and no slippage sections inside the cable.

In the last part of this chapter, the expression for the bending energy stored inside a cable with partially rotating coils is derived and it is shown to be dependent on a single variable, " Ω_0 ": the load factor for the first strand of the first coil at the fixed end. There is a definite relationship between the " Ω_0 " and the external load applied at the end of the cable which will be investigated in the next chapter.

CHAPTER FIVE

HYSTERESIS LOOP FOR A CABLE

5.1 INTRODUCTION

From the tests made on the deflection of cables [20], [21], it has been found that a hysteresis loop always occurs when a cable is deflected and the load removed. If the hysteresis characteristics for cables of commercial sizes under various tensions were known, the maximum amplitudes of vibrations could be predicted quite accurately [20]. A hysteresis loop test method described by Claren and Diana [5] gives the possibility of accurate measurements of cable stiffness and of the energy dissipated per cycle.

It is stated by Claren and Diana that although the real damping forces are not known and are worth further investigation, a mathematical assumption of hysteretic damping for bending leads to analytical results sufficiently close to reality for practical use. They further add that it is necessary in the choice of linearized cable stiffnesses and damping coefficients to use the values obtained from cable deformation tests that

are not too different from those that will occur on the real cables under normal working conditions [5].

As the last step in developing the theoretical model discussed in previous chapters, it is shown that the hysteresis loop for a cable can be obtained in terms of the small slipping sections along the cable length. As mentioned before, this is the first and only attempt in the literature available to explain the mechanics of frictional losses in a cable by Vinogradov and Atatekin, [28], [29]. By using the expressions developed for the slippage of strands in Chapter Three and the expression for the change in the stiffness of a cable derived in Chapter Four, the deflection curve for the cable of the specific geometry shown in Figure (1.1) is found. A hysteresis loop is formed by using the deflection curves obtained during loading and unloading of the cable. The energy dissipated by quasi-static loading of a cable for different levels of maximum load is found and the results are compared with those experimentally determined in the literature.

5.2 FIRST STAGE

As a first stage in an attempt to obtain the hysteresis loop, the applied point load at the free end is assumed to change from zero to a maximum within the limits of small strain assumptions. It is also assumed that when the load is zero there is no residual slippage inside the cable which is an impossible condition to obtain in real life even for the cables just rolled out of the manufacturing line in a factory. Nevertheless, the increment work done by quasi-static loading of such a cable can be written as follows (Figure 4.5):

$$\frac{1}{2} \Delta\alpha P_m \Delta y_1 = \Delta W_{b1} + \Delta W_{t1} + \Delta W_{f1} \quad (5.1)$$

where

P_m = maximum value of load applied

$\Delta\alpha P_m$ = incremental load

Δy_1 = incremental displacement of the cable in the first stage

ΔW_{b1} = incremental bending energy stored in the cable

ΔW_{t1} = incremental torsional energy stored in the cable

Wf_1 = incremental friction work done in the cable by interstrand slippage.

To find the incremental frictional work, the following equation can be used:

$$\Delta Wf_1 = \frac{mf}{\cos\lambda} r \sum_{i=1}^{6N} \int_{-\beta_1 i}^{\beta_1 i} \int_{\theta_1(\Omega i)}^{\theta_1(\Omega i + \Delta\Omega i)} d\theta_1 d\beta \quad (5.2)$$

Remembering the symmetry of the slipping section and another set of the slipping sections on the other side of the cable, equation (5.2) can be put into the following form:

$$\Delta Wf_1 = \frac{4}{\cos\lambda} \frac{mf}{\cos\lambda} r \sum_{i=1}^{6N} \int_0^{\beta_1 i} [\theta_1(\Omega i + \Delta\Omega i) - \theta_1(\Omega i)] d\beta \quad (5.3)$$

The expression for $\theta_{1i}(\Omega i)$ was found (equation 3.17) to be:

$$\theta_{1i}(\Omega i) = \frac{mf}{GJ} \frac{r^2}{\cos^2\lambda} [-\Omega i (\cos\beta_1 i - \cos\beta i) - \frac{1}{2} (\beta_1 i^2 - \beta i^2)] \quad (5.4)$$

also, from equation (3.12) for $\alpha = 1$

$$\Omega_{mi} = \frac{T_m' i}{\gamma} \quad (5.5)$$

by using equations (3.13), (3.14) and (3.7):

$$mf = \frac{T_m i \cos \lambda}{\Omega_{mi} r} \quad (5.6)$$

by substituting equation (5.6) into (5.4), and taking

$\beta_{1i}(\Omega_i) \approx \beta_{1i}(\Omega_i + \Delta\Omega_i)$, the following expression can be written:

$$\begin{aligned} \theta_{1i}(\Omega_i + \Delta\Omega_i) - \theta_{1i}(\Omega_i) = \\ \frac{T_m i r}{GJ \cos \lambda} (\cos \beta_i - \cos \beta_{1i}) \frac{\Delta\Omega_i}{\Omega_{mi}} \end{aligned} \quad (5.7)$$

If equation (5.7) is put into equation (5.3) and integrated:

$$\begin{aligned} \Delta W_{f1} = \frac{4 mf r^3 P_m \sin \lambda}{GJ \cos^2 \lambda} \sum_{i=1}^{6N} \frac{\Delta\Omega_i}{\Omega_{mi}} T_m' i (\sin \beta_{1i} \\ - \beta_{1i} \cos \beta_{1i}) \end{aligned} \quad (5.8)$$

Which gives the work lost in friction inside a cable during the first stage of loading.

The expression for incremental torsional energy can be written as:

$$\Delta W_{t1} = \frac{r}{2 GJ \cos \lambda} \sum_{i=1}^{6N} \int_{-\beta_1 i}^{\beta_1 i} [T_i^2 (\Omega_i + \Delta \Omega_i) - T_i^2 (\Omega_i)] d\beta \quad (5.9)$$

where the expression for net internal torque " T_i " at any cross-section can be found as:

$$T_i = \frac{d\theta_{1i}}{ds} = \frac{\cos \lambda}{r} \frac{d\theta_{1i}}{d\beta} \quad (5.10)$$

or

$$T_i(\Omega_i) = \frac{mf r}{GJ \cos \lambda} (-\Omega_i \sin \beta_i + \beta_i) \quad (5.11)$$

by taking $\beta_i(\Omega_i) \approx \beta_i(\Omega_i + \Delta \Omega_i)$ and using equation (5.6):

$$T_i^2(\Omega_i + \Delta\Omega_i) - T_i^2(\Omega_i) = 2 T_{mi}^2 (\Omega_i \sin^2\beta_i - \beta_i \sin\beta_i) \frac{\Delta\Omega_i}{\Omega_{mi}^2} \quad (5.12)$$

Again by considering the symmetry of the slipping section and another set of slipping sections on the other side of the cable, equation (5.12) is put into (5.9) and integrated to obtain the expression for incremental torsional energy as:

$$\Delta W_{t1} = \frac{P_m^2 r^3}{GJ \cos\lambda} \sum_{i=1}^{6N} \frac{T_{mi}^2 \sin^2\lambda \Delta\Omega_i}{\Omega_{mi}^2} [\Omega_i (2\beta_{1i} - \sin 2\beta_{1i}) + 4 \beta_{1i} \cos\beta_{1i} - 4 \sin\beta_{1i}] \quad (5.13)$$

by further remembering equation (5.5):

$$\Omega_{mi} = \frac{T_{m'i}}{\gamma} \quad (5.14)$$

and equation (3.12):

$$\Omega_i = \alpha \frac{T_{m'i}}{\gamma} \quad (5.15)$$

or:

$$\Delta\Omega_i = \Delta\alpha \frac{T_m' i}{\gamma} \quad (5.16)$$

it can be seen that:

$$\frac{\Delta\Omega_i}{\Omega_{mi}} = \Delta\alpha \quad (5.17)$$

Equation (5.17) is not dependent on strand number "i" and can be taken out of the summation sign in equation (5.13). Equation (5.13) can be written as follows:

$$\begin{aligned} \Delta W_{t_i} = \frac{P_m^2 r^3}{GJ \cos\lambda} \left(\frac{\Delta\Omega}{\Omega_m} \right)^2 \sum_{i=1}^{6N} \frac{T_m' i \sin^2\lambda}{\Delta\Omega_i} [\Omega_i (2\beta_1 i \\ - \sin 2\beta_1 i) + 4\beta_1 i \cos\beta_1 i - 4 \sin\beta_1 i] \quad (5.18) \end{aligned}$$

Incremental bending energy stored in the cable can be written by substituting the expression for incremental

load: $\Delta P = \Delta \alpha P_m$ into equation (4.36), expressing from equation (5.17) and using $h = 2\pi r N \tan \lambda$

$$\begin{aligned} \Delta W_{b1} = & \frac{P_m^2 r^3}{2 EI_w} \left(\frac{\Delta \Omega_o}{\Omega_m} \right) \left\{ 8\pi^3 N^3 \tan^3 \lambda \left[\frac{x_1^3}{165} \right. \right. \\ & + \frac{(1-x_2^3)}{21} - \frac{(x_2^2-x_1^2)}{2 C_2} - \frac{C_1}{C_2} (x_2 - x_1) \\ & \left. \left. - \frac{C_1^2}{C_2^3} \ln \frac{(C_1 - C_2 x_2)}{(C_1 - C_2 x_1)} \right] \right\} \end{aligned} \quad (5.19)$$

where C_1, C_2, x_1, x_2 are as defined in equations (4.37)-(4.42).

After having obtained all the energy terms, equations (5.19), (5.18) and (5.3) can be put into (5.1) and simplified by using the following expressions:

$$\Delta \alpha = \frac{\Delta \Omega_o}{\Omega_m} \quad (5.20)$$

$$GJ = \frac{EI_w}{(1+\mu)} \quad (5.21)$$

to obtain:

$$\Delta y_1 = \left(\frac{\Delta \Omega_0}{\Omega_m} \right) \frac{P_m r^3}{EIw} \left\{ 8\pi^3 N^3 \tan^3 \lambda \left[\frac{x_1^3}{165} + \frac{(1-x_2^3)}{21} - \frac{(x_2^2-x_1^2)}{2 C_2} \right. \right.$$

$$\left. - \frac{C_1}{C_2} (x_2-x_1) - \frac{C_1^2}{C_2^3} \ln \frac{(C_1-C_2 x_2)}{(C_1-C_2 x_1)} \right] + \frac{(1+\mu)}{\cos \lambda} \sum_{i=1}^{6N} T_m' i^2 \frac{\sin^2 \lambda}{\Delta \Omega_i} [\Omega_i (2\beta_{1i}$$

$$- \sin 2\beta_{1i}) + 4 \beta_{1i} \cos \beta_{1i} - 4 \sin \beta_{1i}]$$

$$+ \frac{16 \sin^2 \lambda (1+\mu) \pi N}{\Delta \Omega \cos \lambda} \sum_{i=1}^{6N} T_m' i (\sin \beta_{1i} - \beta_{1i} \cos \beta_{1i}) \quad (5.22)$$

with:

$$C_1 = 273.18 \quad (5.23.a)$$

$$C_2 = 218.18 \Omega_0 \quad (5.23.b)$$

$$x_1 = x_2 = 1 \quad \text{for } 0 \leq \Omega_0 \leq 1 \quad (5.23.c)$$

$$x_1 = A' \quad x_2 = 1 \quad \text{for } 1 \leq \Omega_0 \leq 1.22 \quad (5.23.d)$$

$$x_1 = A' \quad x_2 = B' \quad \text{for } 1.22 \leq \Omega_0 \quad (5.23.e)$$

$$A' = 1/\Omega_0 \quad (5.23.f)$$

$$B' = 1.22/\Omega_0 \quad (5.23.g)$$

where:

$$\Omega_0 = \frac{\alpha P_m \pi N \sin^2 \lambda}{mf} \quad (5.24)$$

or:

$$\Omega_0 = \alpha \Omega_m \quad (5.25)$$

or by using $h = 2\pi r N \tan \lambda$, equation (5.24) can be written as:

$$\Omega_0 = \frac{\alpha P_m h \cos^2 \lambda}{mf r} \quad (5.26)$$

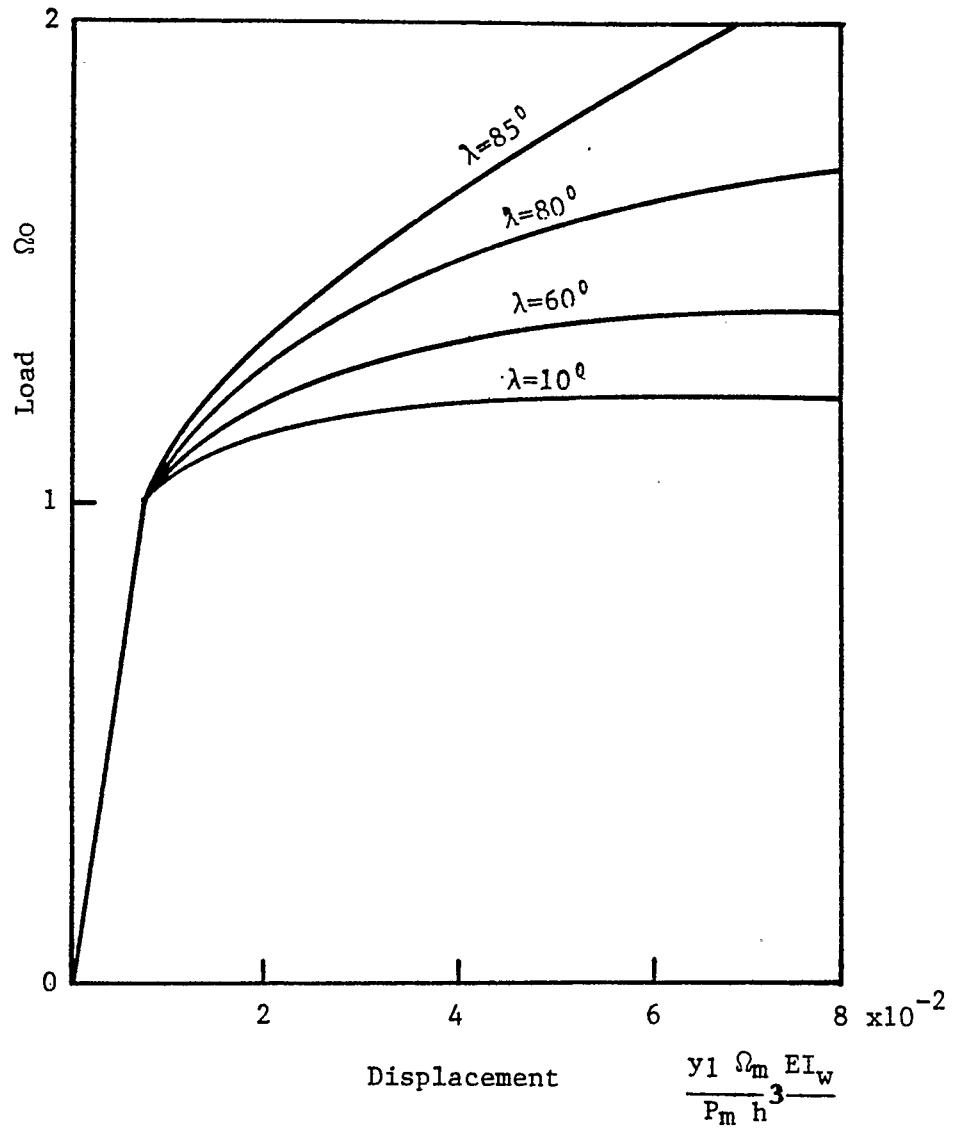


Figure (5.1) Theoretically Obtained Deflection Curve for a Cable.

An algorithm for solving equation (5.22) together with equations (5.23), (4.5), (4.7.b), (4.8) and (4.9) is given in the Appendix III. A careful examination of equation (5.22) shows that dimensionless displacement parameter "Y" is a function of " λ " and "N". However, solution of equation (5.22), Figure (5.1), shows no significant sensitivity to the maximum number of coils in the cable. Also for $10^0 \leq \lambda < 60^0$, the deflection curve is insensitive to the change in " λ " too. For $\lambda \geq 60^0$ the deflection curve and the amount of maximum deflection changes dramatically with changes in λ .

5.2.1 SOME PRACTICAL APPLICATIONS

Since it is difficult to visualize the load-deflection curve for a cable in terms of " Ω " v.s. $(y_1 \Omega_m EI_w / P_m h^3)$, a practical way of obtaining load-deflection curves in terms of Force vs. Displacement will be explained below. It is assumed that all the physical characteristics of the cable (i.e. $h, r, r_w, \lambda, E, I_w, m_f$) and the maximum value of the applied load (P_m) is known. Then the maximum load coefficient (Ω_m) can be found as follows:

$$\Omega_m = \frac{P_m h \cos^2 \lambda}{m_f r} \quad (5.27)$$

For any $0 \leq \Omega_0 \leq \Omega_m$, from Figure (5.1):

$$\frac{y_1 \Omega_m EIw}{P_m h^3} \Big|_{\Omega = \Omega_0} = C_1 \quad (5.28)$$

Then, load and displacement for that particular Ω_0 can be found as:

$$y_1 = C_1 \frac{P_m h^3}{EIw \Omega_m} \quad (5.29)$$

$$P = P_m \frac{\Omega_0}{\Omega_m} \quad (5.30)$$

A load-deflection curve obtained for a specific case is shown in Figure (5.2).

5.3 SECOND STAGE

In the second stage of loading, applied load is assumed to be changing from maximum to minimum (i.e. $1 \geq \alpha \geq -1$). As it has been explained in Section 3.4, by means of the transformations:

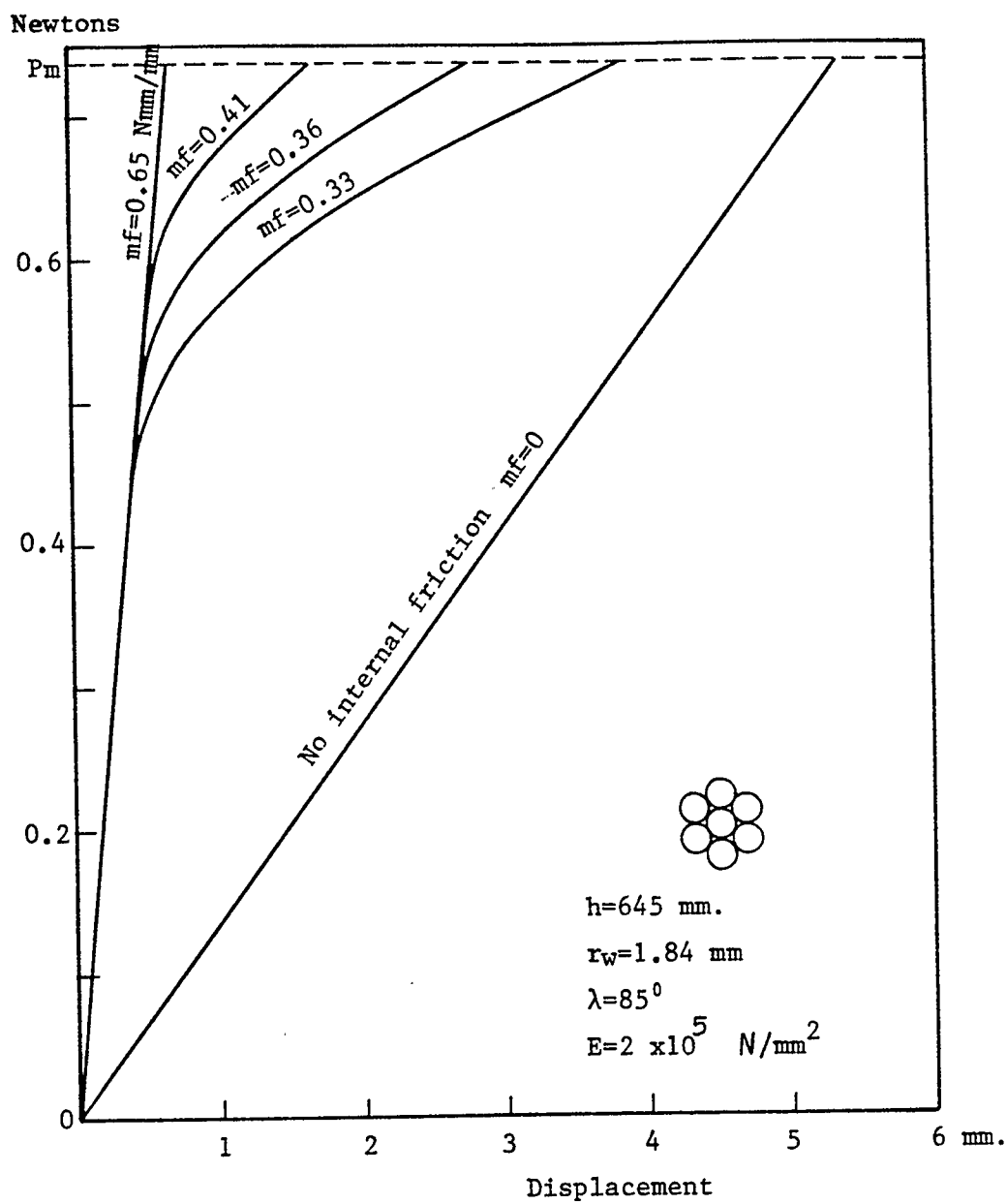


Figure (5.2) Deflection Curve for a Specific Case.

$$\Omega_i = \Omega_{mi} - 2\Omega_{i^*} \quad (5.31)$$

$$\eta_{2i} = \eta_{mi} - 2\eta_{i^*} \quad (5.32)$$

the expressions for the slippage angle and the boundary length for the slipping section at any strand can be expressed as:

$$\eta_{i^*} = \Omega_{i^*} (\cos\beta_i - \cos\beta_{1i}) + \frac{1}{2} (\beta_i^2 - \beta_{1i}^2) \quad (5.33)$$

$$\Omega_{i^*} \sin\beta_{1i} - \beta_{1i} = 0 \quad (5.34)$$

for which:

$$0 \leq \Omega_{i^*} \leq \Omega_{mi} \quad (5.35)$$

By comparing the equations (5.33), (5.34) and (5.35) to equations (3.11.a,b) and (3.17), it can be seen that they are identical. Since the amount of slippage at any cross-section, boundaries of the slipping sections and the amount of load-applied have the same range and the same minimum and maximum values, it can be seen that, in terms of (*) coordinates, the following expressions can be written for the second stage:

$$\Delta W_{b2}^* = \Delta W_{b1} \quad (5.36)$$

$$\Delta W_{t2}^* = \Delta W_{t2} \quad (5.37)$$

$$\Delta W_{f2}^* = \Delta W_{f2} \quad (5.38)$$

The expression for the second-stage in terms of (*) coordinates for the incremental work done by quasi-static loading of a cable can be written as:

$$\frac{1}{2} \Delta \alpha_{Pm} \Delta y_2^* = \Delta W_{b2}^* + \Delta W_{t2}^* + \Delta W_{f2}^* \quad (5.39)$$

If equations (5.36), (5.37) and (5.38) are put into (5.39) and compared with (5.1) it can be seen that:

$$\Delta y_2^* = \Delta y_1 \quad (5.40)$$

for:

$$\Omega_0^* = \Omega_0 \quad (5.41)$$

Therefore, by using the transformations (5.31) and (5.32), the real displacement and load for the cable in the second stage can be found by:

$$y_2 = y_m - 2y_2^* \quad (5.42)$$

$$\Omega_2 = \Omega_m - 2\Omega_0^* \quad (5.43)$$

Then the same equations and the algorithm developed for the first stage of the hysteresis loop can be used to find the load-deflection curve for the second stage. Hysteresis loops obtained by using above equations for different values of helix angle " λ " and maximum load coefficient " Ω_m " are shown in Figure (5.3) and Figure (5.4).

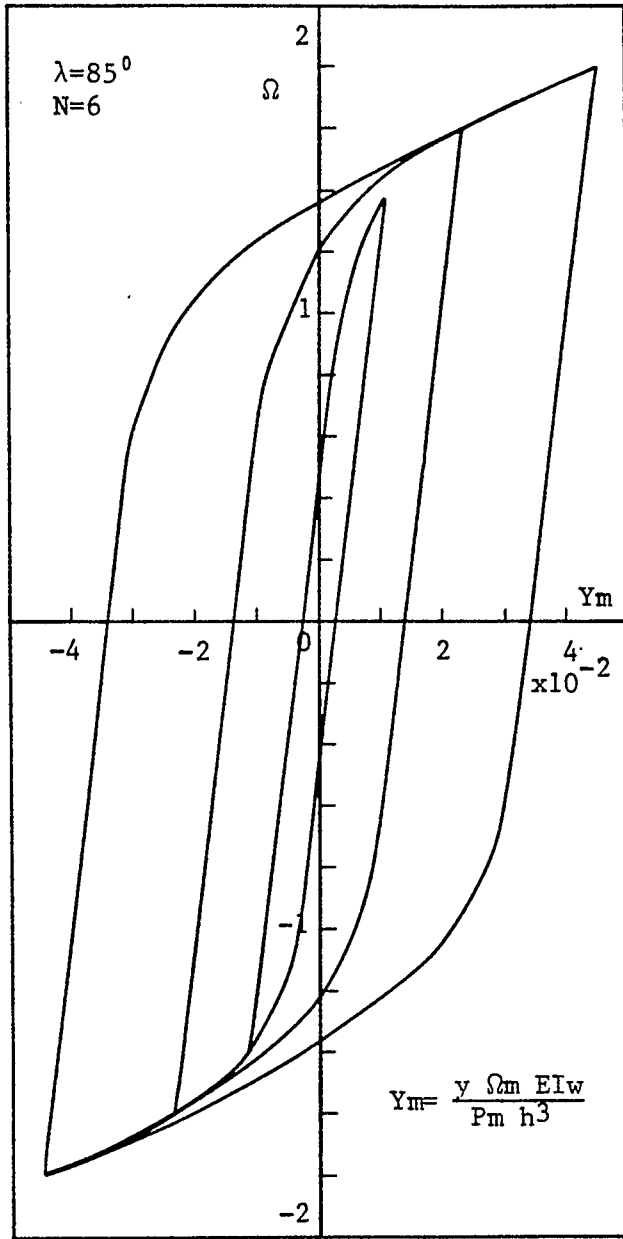


Figure (5.3) Hysteresis Loop for a Cable.

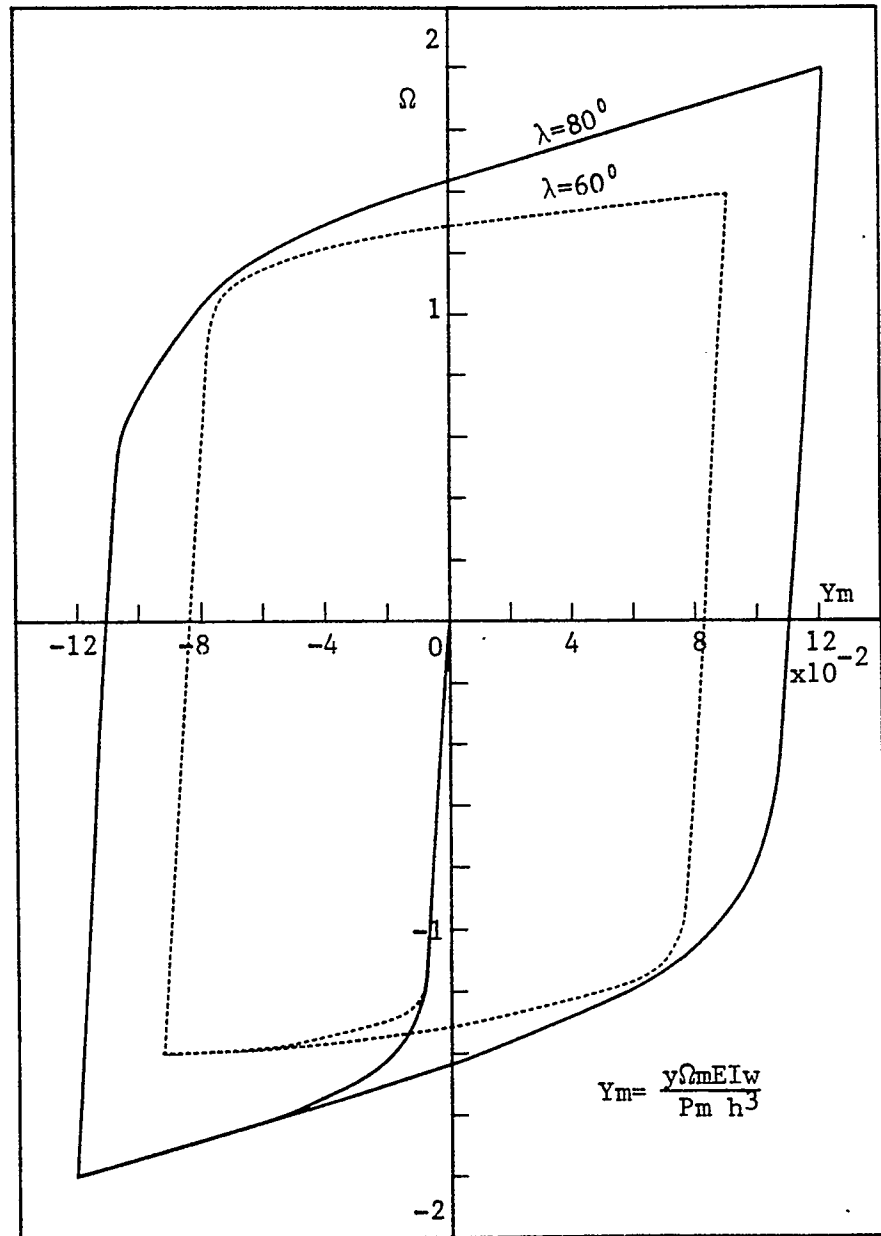


Figure (5.4) Hysteresis Loop for a Cable.

5.4 COMPARISON WITH EXPERIMENTAL RESULTS

The hysteresis loop obtained from the experiments on a steel cable is shown in Figure (5.5). In order to compare the hysteresis loop of Figure (5.5), first, an imaginary curve for first stage is drawn on Figure (5.5) by making use of the experimentally obtained curve for second stage (i.e. stiffness of the cable is the same in the beginnings of first and second stages as there is no internal slippage until $\Omega_0 = 1$).

It can be found that the at approximately $\alpha \cong 0.20$, the stiffness of the cable starts to change, for which $\Omega_0 = 1$, then from equation (5.26):

$$mf = \frac{\alpha P_m h \cos^2 \lambda}{\Omega_0 r} \quad (5.44)$$

for $\Omega_0 = 1$, $\alpha \cong 0.20$, $P_m = 2.55 \text{ N}$, $h = 644.5 \text{ mm}$, $r = 5.52 \text{ mm}$, $\lambda = 85^\circ$

$mf = 0.45 \text{ N}\cdot\text{mm}/\text{mm}$ can be found.

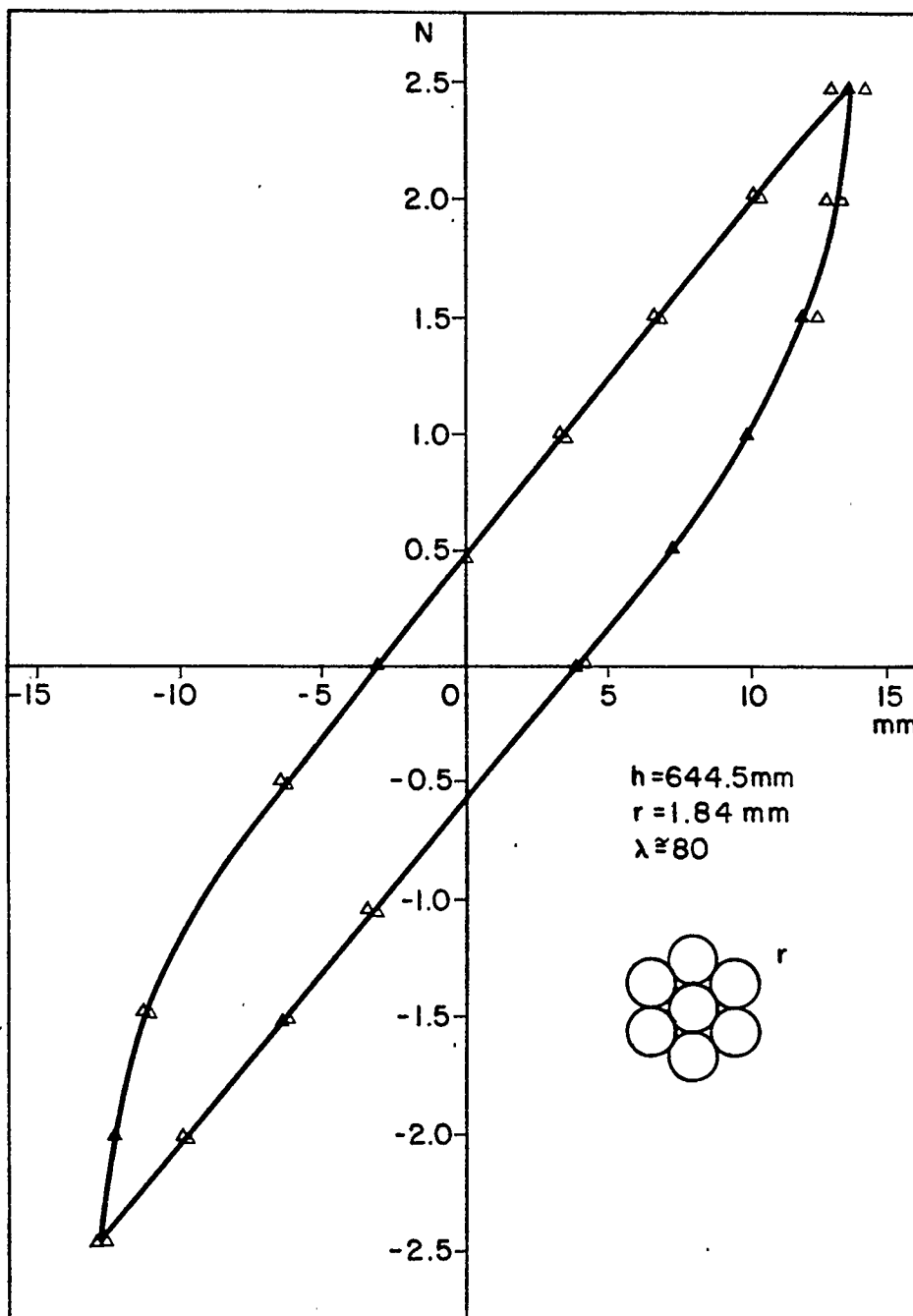


Figure (5.5) Experimentally Found Hysteresis Loop
for a Cable.

Then, again from equation (5.26) for $\alpha = 1$:

$$\Omega_m = \frac{P_m h \cos^2 \lambda}{m f r} \quad (5.45)$$

$$\Omega_m = 5.0$$

is obtained.

From Figure (5.1) for $\lambda = 85$ and $\Omega_m = 5.0$, the maximum displacement can be found as:

$$\frac{y_m \Omega_m EIw}{P_m h^3} = 0.4$$

or:

$$y_m = 25 \text{ mm}$$

When compared with: $y_{m \text{ exp}} = 13 \text{ mm}$ (92% error)

The 92 % error found above can be explained in terms of the uneven friction forces along the cable. It has been mentioned before that the coils start slipping at the clamped end. In theoretical calculations, it is assumed that the internal friction force is constant all along the cable including the close vicinity of the clamped end. In real life, however, clamping increases the magnitude of the friction forces inside the cable. Since this increase in friction forces is limited to the close vicinity of the

clamped end, the length of the slipping section decreases and the cable becomes stiffer.

It can be proven that the discrepancy between the theoretical and experimental values of cable stiffness are dependent on the magnitude of clamping forces, cable geometry and initial friction force between the strands.

5.5 INTERNAL LOSS IN A CABLE

Areas of the hysteresis loops shown in Figures (5.3) and (5.4) give the amount of energy dissipated by friction forces inside a cable. If the area of each hysteresis loop is found and plotted with respect to maximum displacement obtained for that particular hysteresis loop, then a straight line as shown in Figure (5.6) is obtained.

Before discussing the relationship between dissipated energy and displacement any further, a quick review of the two most common types of damping proves to be useful.

Coulomb damping is a non-linear damping phenomenon, since discontinuities exist in the damping force time history when a change in the direction of relative velocity occurs, thereby resulting in a non-linear equation of motion. The Coulomb damping force is of constant magnitude and is independent of displacement. In a physical sense,

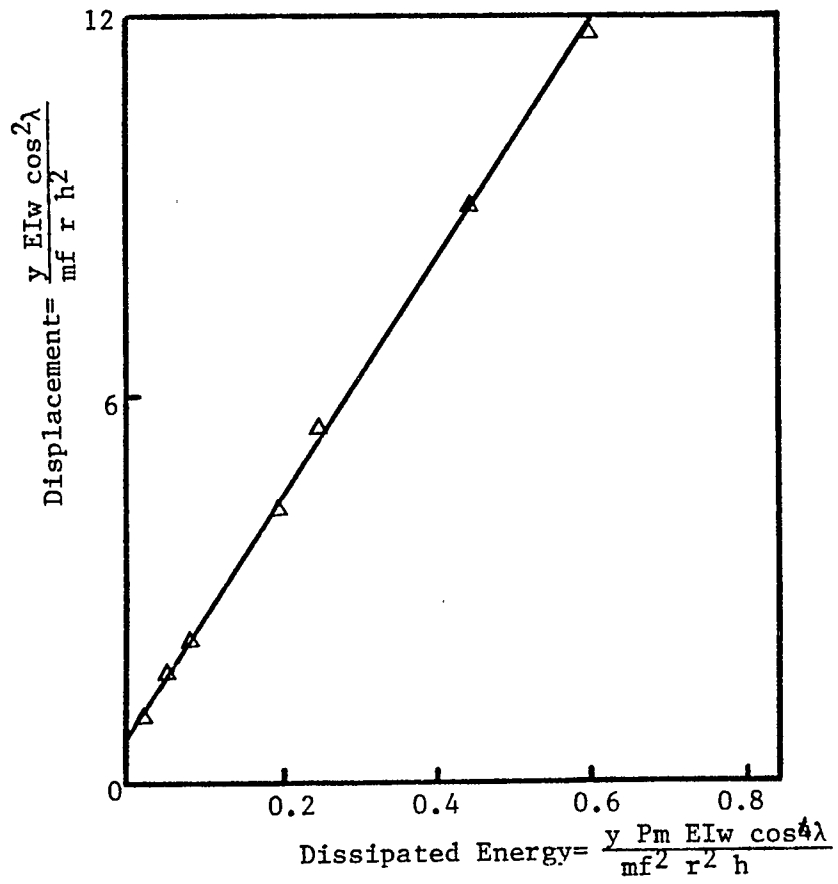


Figure (5.6) Energy Dissipated per Cycle as a Function of Maximum Displacement.

Coulomb damping is attainable from a relative motion of two surfaces arranged to slide one upon the other with a constant normal force holding them together, where the coefficient of friction between the two surfaces is primarily dependent on the nature of the surfaces sliding on each other. The energy dissipated per cycle by a Coulomb damper experiencing a harmonic relative displacement is independent of the frequency of vibration amplitude [27].

Hysteretic damping is a linear damping phenomenon for which the damping force is proportional to the relative displacement across the damper, where the constant of proportionality is defined as the hysteretic damping coefficient.

The concept of hysteretic damping was originally postulated as a basis for describing the internal damping properties of solid materials. From a rigorous mathematical point of view, hysteretic damping does not represent a physically realizable energy dissipation mechanism since the response may anticipate excitation under some circumstances [27]. It is used, however, to represent the internal damping characteristics of solid materials undergoing harmonic vibrations. In a conceptual sense, hysteretic damping is attainable from a viscous

The energy dissipated per cycle by a hysteretic damper experiencing a harmonic relative displacement is independent of the frequency of the vibration but depends on the vibration amplitude.

Remembering the assumption of Coulomb damping for inter-strand friction (Section 3.1), the first degree curve obtained in Figure (5.6) proves that the expressions obtained for the slippage of cross-sections and the hysteresis loop obtained for a cable are correct as far as the assumptions made about the nature of losses in a cable are concerned.

Claren and Diana [5] mentioned that the energy dissipated per cycle is not proportional to the square of the displacement of the end of the cable as it would have been in the case of hysteretic damping (see Figure 5.7), nor directly proportional to displacement as it would have been in the case of Coulomb damping. The energy dissipated lies in between the two theoretical curves as shown in Figure (5.7). It is also stressed, however, that the energy can be dissipated without macroscopic slippage of strands, by the deformation of microscopic interstrand asperities.

In another paper by Sturm [20], measurements are made for the energy dissipated in the steel cable of a

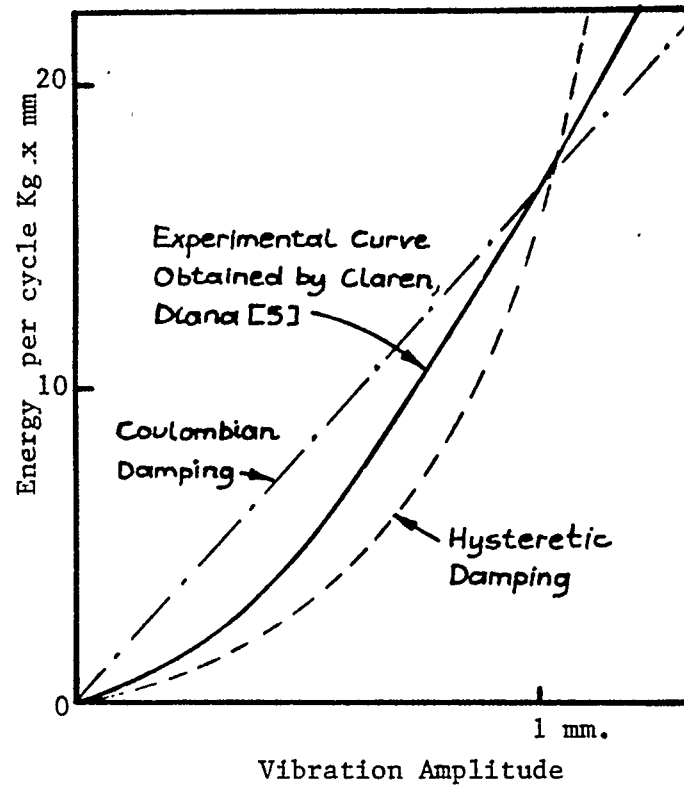


Figure (5.7) Comparison of the Experimental Energy Dissipation Curve with the Theoretical Curves.

Stockbridge damper and the resulting curve is compared with a hysteretic damping curve.

By also noting the obvious discrepancy between Sturm's experimental Energy loss curve and the theoretical curve y

$= kX^2$ it can be seen that the internal damping of cables can be explained in terms of two different mechanisms:

1. Coulomb friction between the strands inside a cable.

2. Hysteretic damping resulting from the deformation of the individual strands and microscopic interstrand asperities.

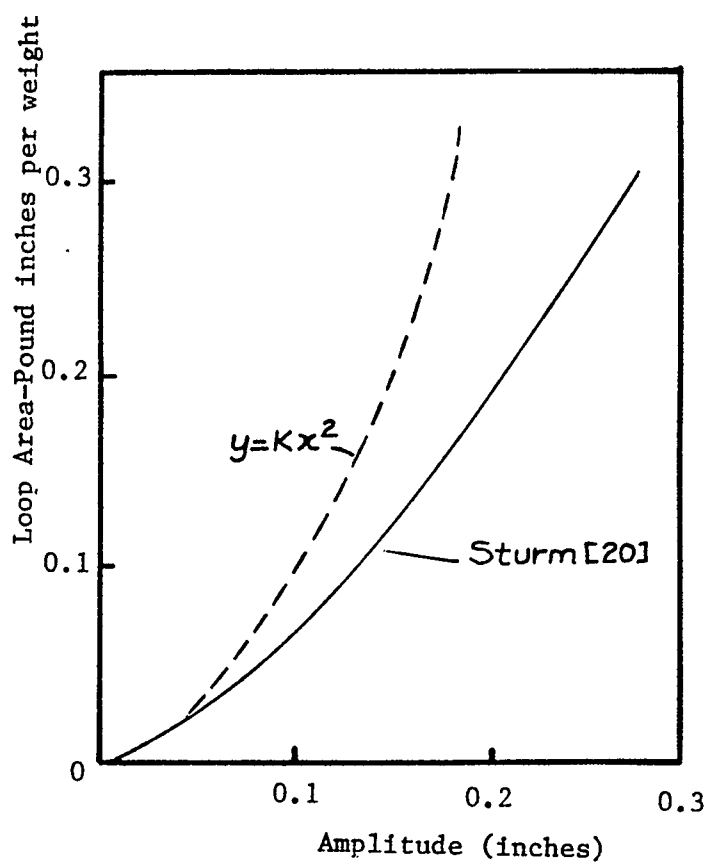


Figure (5.8) Loss v.s. Deflection Curve by Sturm [20].

Although in most papers published in this field an assumption of hysteretic damping is made [20], [5], [6], [7], in a paper by Carroll [21], the amount of energy taken from the wind by the vibrating cable is measured by means of a coil in a magnetic field and it is shown that energy taken is proportional to the displacement.

It can be reasoned that for cables made from materials with comparatively lower values of Young's Modulus, within the limit of small strains, the energy spent on deformation of strands would be less than the energy spent on the Coulombian friction between the strands.

The non-dimensional term for the dissipated energy Ψ can be written as follows:

$$\Psi = Y_1 \Omega_m \quad (5.45)$$

where:

Y_m = non-dimensional displacement (Y_{1max})

$$Y_m = \frac{y_m EIw \cos^2 \lambda}{mf h^2 r} \quad (5.46)$$

Ω_m = non-dimensional load

$$\Omega_m = \frac{P_m h \cos^2 \lambda}{m f r} \quad (5.47)$$

by putting equations (5.47) and (5.46) into equation (5.45):

$$\Psi = \frac{y_m P_m E I_w \cos^4 \lambda}{m f^2 r^2 h} \quad (5.48)$$

together with equation (2.2.a):

$$h = 2\pi r N \tan \lambda \quad (5.49)$$

$$\Psi = \frac{y_m P_m E I_w \pi^2 N^2 \sin^2 2\lambda}{m f^2 h^3} \quad (5.50)$$

It can be seen from equation (5.50) that energy dissipated increases with an increase in "y_m", "P_m", "E I_w" and "N". However, as "h" is increased, everything else being kept the same, dissipated energy decreases as for a constant number of turns "λ" changes, coils become flatter and the torsional moment at any cross-section decreases.

If equation (5.50) is written as:

$$\Psi = \frac{C_1}{m f^2} \quad (5.51)$$

and differentiated:

$$\Delta\Psi = -2 \frac{C_1}{mf} \Delta mf \quad (5.52)$$

Which shows that with an increase in the interstrand friction torque, the amount of dissipated energy decreases, as the coils slip less and the cable deflects less (for constant applied force P_m). This change in the energy lost is greater at smaller values of friction.

As was shown before in equation (2.30):

$$y_m \propto \frac{P_m h^3}{EIw} \quad (5.53)$$

If equation (5.53) is put into equation (5.50):

$$\Psi \propto \left(\frac{P_m}{mf} \right)^2 N^2 \sin^2 \lambda \quad (5.54)$$

Which shows that it is the ratio (P_m/mf) , rather than P_m , or mf that is important in analyzing the internal losses in the cable. Again from equation (5.54), it can be seen that the energy lost is a maximum for $\lambda = 45^\circ$.

5.6 CONCLUSION

In this chapter, expressions for the internal energy stored in the cable and the friction work done are written for two stages of loading at the free end of the cable. Equations derived for the slippage of strands in Chapter Three are used to obtain the internal energy stored in the rotation of the strands and the friction work lost by the slippage. A quasi-static approach is used and the external load is applied in small increments. The resulting bending energy is obtained from the equations developed in Chapter Four and it is shown that the deflection curve for a cable, in terms of non-dimensional quantities, is very sensitive to the changes in the helix angle " λ ", for $\lambda \geq 60^\circ$.

In section 5.3 it is shown that by using a certain transformation the deflection curve for the second stage of loading of a cable can be derived from that of the first stage by combining the first and second stage of loading, knowing that the third stage is a symmetry of the second stage. Hysteresis loops for various values of load factor (Ω_m) and (λ) are obtained and shown in Figures (5.3) and (5.4). By plotting the areas of hysteresis loops (energy lost) versus displacement it is shown that the

non-dimensional energy lost " ψ " is proportional to non-dimensional maximum displacement " Y_m ", as could be predicted from the assumption of Coulomb friction between the strands inside a cable.

Theoretically found lost energy versus displacement curve is compared with those found in the literature and it is shown that the slippage mechanism developed in this thesis accounts for one of the two ways a deflected cable loses internal energy. Therefore the first degree lost energy versus displacement curve shown in Figure (5.6) constitutes a limiting case for the actual lost energy versus displacement curves obtained from the experiments (Figure 5.7).

Hysteretic damping resulting from the deformation of the individual strands and microscopic asperities is the other way cables lose internal energy. In many publications [5], [6], [7], [20], [21], the actual behaviour is shown to be somewhere between (Figure 5.7) the two extremes mentioned above.

In almost all the publications, however, hysteretic damping is assumed to explain the losses inside the cables, and loosening and slippage of strands treated as something that affects the stiffness of the cable in an unknown way [5].

In this chapter, the contribution of strand slippage to the internal loss of a cable is investigated and it is shown that an increase in the ratio (P_m / m_f) and total number of coils (N) increases the energy lost which is also a maximum for a 45° helix angle.

CHAPTER SIX

GENERAL DISCUSSIONS AND CONCLUSIONS

In this thesis a simple three dimensional model for the cable is developed to explain the internal losses in the cables. As the simplest model that has all the characteristics of the actual cable structure, a helical spring wound around a cylindrical core is considered (Figure 2.1).

Out of the two possible ways of slippage between the coil (spring) and the core (i.e. rotation and translation), in Chapter Two, it is shown that the deflected centerlines for the coil and the core coincide which rules out the possibility of interstrand translation as a major form of slippage, Vinogradov and Atatekin [29], [28]. Having decided that the rotation of coils is the principal form of energy dissipation, the existence and significance of such rotations were measured by means of a Rotation Measuring Device (RMD) on a "free" helical coil that had no internal core. Experimentally measured values of rotations were then compared and found to be in good agreement with the theoretical results. (Table 1).

Noting the periodic nature of twisting moment and rotation angle at any cross-section and of the coil

structure, a section of the coil core model is isolated from the rest of the model to be analyzed separately in Chapter Three. A mathematically equivalent physical model as shown in Figure (3.2) is used to explain the losses inside the cables in terms of small slipping sections along the coil length, Vinogradov and Atatekin [28].

Uniformly distributed friction torque is assumed to exist between the coil and the core, but if the coil does not rotate, friction torque is assumed to be zero. The applied load changes from zero to a maximum in the first stage and from a maximum to a minimum in the second stage.

It is shown that the slippage starts as the internal twisting moment gets bigger than the friction torque at some cross-section (ϕ_{mi}) and propagates in either direction on the coil, thereby forming a slipping section of finite length. Due to the change in the sign of the twisting moment the maximum length of such slipping sections are found to be half the length of a coil. In Chapter Three, also the expressions for the location of the center of such slipping sections, the distribution of slippage and the propagation of boundary length are given for stages one and two, and the expressions for stage three are shown to be identical to the ones for stage two with a reversal of signs.

With the help of a set of transformation equations (3.34) and (3.35), it is also shown that the amount and the boundary of slippages for stage two can be found from those of the first stage. The hysteresis loop obtained in terms of the non-dimensional load factor (Ω) and the slippage term (η) , (Figure 3.3) is valid for any cross-section of any strand of any cable made of any number of strands.

By designing a 20 times more sensitive Rotation Measuring Device, measurements were done at different cross-sections of an auto shock spring with a bicycle inner tube connected to a hydraulic pump to change the pressure and therefore the friction torque on the coils. Experimentally drawn hysteresis loops are found to be qualitatively the same as the theoretical one of Figure (3.3).

Having obtained the basic relationships between the twisting torque and the slippage at a small section in Chapter Three, the next step is to find the response of all such slipping sections as a whole and to obtain a general way of describing those sections in a cable with six strands wound around a central core. In Chapter Four, boundaries of the slipping sections expressed in local coordinates are transformed and expressed in terms of the global coordinates of the cable. Using the expression found for the boundary of all such slipping sections, the

number of slipping strand cross-sections are determined at each cross-section, to develop a model for the "loosening" of the cable under the applied load.

By introducing a critical load factor (Ω_0), which is the value of Ω at the first strand of the first coil for any applied load at the end of the cable, it is shown that for $\Omega_0 \leq 1$, there is no slippage at any cross-section of the cable and $I/I_w = 55$ for $0 \leq z \leq h$. For $1 \leq \Omega_0 \leq 1.22$, the clamped end of the cable starts to slip partially without any complete slippage and the boundary of partial slippage "A" can be found from $A = 1 - 1/\Omega_0$. For $\Omega_0 > 1.22$, all three sections of complete slippage, partial slippage and complete non-slippage can be found inside a cable and the boundary of complete slippage "B" can be found from the expression $B = 1 - 1.22 / \Omega_0$. $I/I_w = 7$ for a completely slipping part of the cable and the expression for a partially slipping section is given by equation (4.33.b).

In Chapter Five, the incremental work done on a cable by quasi-static loading is found by using the expressions for incremental bending and torsional energies stored in the cable and incremental friction work lost by strand slippage. Once again the load is applied in two stages; and the expressions found in Chapter Three for the amount

and the boundary of the slippage, are used in developing the incremental torsional energy and the friction work equations of Chapter Five. The incremental bending energy term is obtained by making use of the expressions developed in Chapter Four to describe slippage along the coil. Solving the resulting equation numerically, hysteresis loops for cables with different values of helix angle (λ), maximum load factor (Ω_m) and total number of coils (N) are obtained. It is shown that in term of non-dimensional variables, the maximum displacement does not depend on " N " but is greatly affected by the changes in " λ ", especially for $\lambda \geq 60^\circ$.

The hysteresis loop found from the tests conducted on a steel cable of commercial size is compared with the theoretical one and found to be in good qualitative agreement. From a comparison of experimentally and theoretically obtained hysteresis loops, it is found that the clamping forces change the magnitude of the friction forces in their immediate vicinity, which also happens to be the most critical section of the cable.

A consideration of the clamped end of the cable with modified friction forces and more exact boundaries of slippage should be useful to obtain a more exact deflection curve for cables.

As a further step in analysis, areas of hysteresis loops for various values of " Ω_m " and " λ " were found and plotted with respect to maximum displacement " Y_m " (Figure 27). In accordance with the earlier assumption of Coulomb Friction between the strands, a straight line relationship is found between the energy dissipated (Ψ) and the maximum displacement. When compared with those of experimentally found curves in the literature [5], [6], [7], [20], [21], it can be seen that the energy dissipated versus displacement curve found in Chapter Five represents an extreme case of dissipation of internal energy solely by interstrand friction. The real behaviour of the cable, however, is one of a combination of interstrand friction and the deformation of the individual strands and microscopic interstrand asperities as clearly demonstrated by Claren and Diana [5] in Figure (5.7).

In a later part of Chapter Five, at least for the Coulombian part of the energy dissipation, it is shown that the energy dissipated is proportional to the square of the number of coils (i.e. length) and the ratio (P_m / m_f). Energy dissipated is also shown to be maximum for $\lambda = 45$ and decreases with an increase in λ .

During the experiments, due to stock parts (i.e. cable, autospring) displaying great inconsistencies in geometrical dimensions, it was with great difficulty that

consistent and reliable data could be obtained. Especially the assumption of uniform friction torque between the strands proved to be the most difficult to realize under laboratory conditions. Constrained by time and money, little could be done to improve the experimental set-ups to obtain better results.

It is the author's suggestion that before pursuing any more serious theoretical work in this area, experiments described in Chapter Three should be repeated with a custom made spring made to very tight tolerances and a new Rotation Measuring Device using the principle of two polarized planes and a light source instead of mechanical contacts. Also, an automatic loading device instead of a manual one as used by the author could prove to be useful in loading for 1000-2000 cycles to obtain more uniform friction forces before making any measurements.

REFERENCES

1. Love, A.E.H. "A Treatise on the Mathematical Theory of Elasticity", Dover Publications, Inc. New York, N.Y. 1944.
2. Prescott, J. "Applied Elasticity", Dover Publications, Inc., New York, N.Y. 1961.
3. Timoshenko, S. "Strength of Materials, Part II", 3rd Ed., D. Van Nostrand Company, Inc., New York, N.Y. 1956.
4. Machida, S. and Durelli, A.J., "Response of a Strand to Axial and Torsional Displacements", Journal of Mechanical Engineering Science, Vol.15, No.4, 1973, pp.241-251.
5. Claren, R. and Diana, G., "Mathematical Analysis of Transmission Line Vibration", IEEE Transactions on Power Apparatus and Systems, Vol.pas-88, No.12, December 1969.
6. Wagner, H., Ramamurti, V., Sastry, R.V.R. and Hartmann, K., "Dynamics of Stockbridge Dampers", Journal of Sound and Vibration, Vol.30(2), 1973, pp.207-220.
7. Claren, R. and Diana, G., "Dynamic Strain Distribution on Loaded Stranded Cables", IEEE Transactions on Power Apparatus and Systems, Vol.Pas-88, No 11, Nov., 1969, pp.1678-1690.
8. Dhotarad, M.S., Ganesan, N. and Rao, B.V.A. "Transmission Line Vibrations", Journal of Sound and Vibration 60 (2), 1978, pp.217-237.
9. Costello, G.A. and Phillips, W., "Effective Modulus of Twisted Wire Cables", Journal of the Engineering Mechanics Division, ASCE, February, 1976, pp.171-181.
10. Huang, N.C., "Finite Extension of an Elastic Strand with a Central Core", Transactions of the ASME, Vol.45, December 1978, pp.852-858.
11. Phillips, J.W. and Costello, G.A., "Contact Stresses in Twisted Wire Cables", Journal of the Engineering Mechanics Division, ASCE, April, 1973, pp.331-341.

12. Costello, G.A. and Miller, R.E. "Lay Effect of Wire Rope", Journal of the Engineering Mechanics Division, ASCE, August 1979, pp.597-608.
13. Westinghouse Electrical Engineering Handbook, Chapter 3, 1936, pp.32-53.
14. Costello, G.A. and Phillips, J.W. "A More Exact Theory for Twisted Wire Cables", Journal of the Engineering Mechanics Division, ASCE, October 1974, pp.1096-1099.
15. Costello, G.A. "Large Deflections of Helical Spring due to Bending", Journal of the Engineering Mechanics Division, ASCE, June 1977, pp.481-487.
16. Andreeva, L.E. "Elastic Elements of Instruments", Israeli Program for Scientific Translations Ltd. 1966, Jerusalem.
17. Popov, E.P. "Introduction to Mechanics of Solids", Prentice-Hall of India, New Delhi, 1976.
18. Pipes, L.A., "Cable and Damper Vibration Studies", AIEE Transactions, Vol.55, 1936, pp.600-614.
19. Sturm, R.G., "Vibration of Cables and Dampers -1", AIEE Transactions, Vol.55, May 1936, pp.455-465.
20. Sturm, R.G., "Vibration of Cables and Dampers-2", AIEE Transactions, Vol.55, June 1936, pp.673-688.
21. Carroll, J.S., "Laboratory Studies of Conductor Vibration", AIEE Transactions, Vol.55, May 1936, pp.543-547.
22. Migliore, H.J. and Webster, R.L. "Current methods for Analyzing Dynamic Cable Response" pp.3-13.
23. Spillers, W., Greenwood, A.N., Eaton, R. "A helical Tape on Cylinder Subjected to Bending", Journal of the Engineering Mechanics Division, ASCE. Vol.109, No.4, August, 1983. pp.1124-1133.
24. Costello, G.A., Butson, G.J. "Simplified Bending Theory for Wire Rope", Journal of the Engineering Mechanics Division, ASCE. Vol.108, April, 1982, pp.219-227.

25. Tadjbakhsh, I.G. "Constant Twist Deformations of Cables", International Journal of Engineering Science, Vol.21, No.3, pp.263-268, 1983.
26. Dawson, T.H. "Continuum Description of Hysteresis Damping of Vibrations", International Journal of Solids Structures, Vol.14, pp.457-464, 1978.
27. Ruzicka, J.E., Derby, T.F., "Influence of Dampers in Vibration Isolation", The Shock and Vibration Information Center, United States Department of Defence 1971, Naval Research Laboratory, Washington D.C.
28. Vinogradov, O.G. and Atatekin, I.S. "Structural Damping of Stranded Cable", Proceedings of Fourth International Conference on Mathematical Modelling, Zurich, 15-17, August, 1983.
29. Vinogradov, O.G. and Atatekin, I.S. "Structural Damping in Vibrating Cable", Abstract, CANCAM 83, May 10-June 3, Saskatoon, Canada.

APPENDIX I

EXPRESSION FOR LATERAL DEFLECTION OF A SPRING

In a book by Andreeva [16] the vertical deflection of a spring subjected to a concentrated load is given as:

$$y = \frac{Ph^3}{3Ab} + \frac{Ph}{As}$$

where for round wire springs:

$$Ab = \frac{h Ed^4 \cos\lambda}{32 D i (2 + \mu \cos^2\lambda)}$$

$$As = \frac{hEd^4}{8D^3i} \frac{1}{1 + \frac{2}{3} \pi^2 \tan^2\lambda + \mu \left(\frac{\pi^2}{3} + \frac{5}{2} \right) \sin^2\lambda}$$

where

d = Diameter of the wire spring is made of

D = Diameter of the spring coils

i = Number of coils

APPENDIX II

BOUNDARIES OF THE SLIPPING SECTION

Remembering the equation (3.11) that gives the boundary of the slipping:

$$\Omega \sin\beta_1 - \beta_1 = 0 \quad (\text{II.1})$$

Solution of equation (II.1) can be found as the intersection of two functions:

$$f_1 = \sin\beta_1 \quad (\text{II.2})$$

$$f_2 = \beta_1 / \Omega \quad (\text{II.3})$$

from which it can be seen that the above two curves intersect at the origin for any value of Ω and $\beta_1 = 0$ is one of the roots of the equation (II.1).

However, $f_2 = \beta_1 / \Omega$ intersects the $\sin\beta_1$ curve at another point of if

$$\left. \frac{df_2}{d\beta_1} \right|_{\beta_1=0} < \left. \frac{df_1}{d\beta_1} \right|_{\beta_1=0} \quad (\text{II.4})$$

which gives

$$\Omega \gg 1 \quad (11.5)$$

as a condition for the start of slippage at the ϕ_m .

Since it is also known that at the end of the slipping section $\beta_1 = \pi/2$, the slope of the line f_2 , for a case of total slippage can be written as:

$$\frac{df_2}{d\beta_1} = \frac{2}{\pi} \quad (11.6)$$

from which

$$\Omega = \frac{\pi}{2} \quad (11.7)$$

is obtained.

Therefore it is proven that the coils start to slip at $\Omega = 1$ for which $\beta_1 = 0$, $\beta_1 \geq 0$ for $\Omega \geq 1$, and $\beta_1 = \pi/2$ for $\Omega \geq \pi/2$ due to the symmetry of loading and geometry. After $\Omega = \pi/2$, any further increase in Ω does not cause an increase in β_1 as it meets the rotation boundary of the next immediate section at $\beta = \pi/2$ which has an equal magnitude of torque acting on it in the reverse direction.

APPENDIX III

ALGORITHM: FOR SOLVING EQUATION 5.22

$$\Omega_0 = 0$$

$$i = 1, 6N$$

$$\phi_{mi} = \tan^{-1} \left[- \frac{1}{2\pi N - (i-1)\pi/3} \right]$$

$$Tm'i = \sin\phi_{mi} - [2\pi N - (i-1)\pi/3] \cos\phi_{mi}$$

$$\Omega_i = \Omega_0 Tm'i / 2\pi N$$

$$\Delta\Omega_i = \Delta\Omega Tm'i / 2\pi N$$

$$\Omega_i \sin\beta_{1i} - \beta_{1i} = 0$$

$$\frac{Tm'i^2 \sin^2\lambda}{\Delta\Omega_i} [\Omega_i(2\beta_{1i} - \sin 2\beta_{1i}) + 4\beta_{1i} \cos\beta_{1i} - 4\sin\beta_{1i}] = \text{SUM } 17$$

$$Tm'i (\sin\beta_{1i} - \beta_{1i} \cos\beta_{1i}) = \text{SUM } 18$$

CONTINUE

$$C_1 = 273.18 \quad C_2 = 218.18 \Omega_0$$

$$x_1 = 1 / \Omega_0 \quad \text{IF } x_1 > 1, x_1 = 1$$

$$x_2 = 1.22 / \Omega_0 \quad \text{IF } x_2 > 1, x_2 = 1$$

$$\frac{\Omega_m y_1 EIw}{P_m r^3} = Y_1 = \Delta\Omega_0 \left\{ 8\pi^3 N^3 \tan^3\lambda \left[\frac{x_1^3}{165} + \frac{(1-x_2^3)}{21} - \frac{(x_2^2-x_1^2)}{2 C_2} \right. \right.$$

$$\left. - \frac{C_1}{C_2} (x_2-x_1) - \frac{C_1^2}{C_2^3} \ln \frac{(C_1-C_2x_2)}{(C_1-C_2x_1)} \right] + \frac{(1+\mu)}{\cos\lambda} \sum_{i=1}^{6N} Tm'i^2 \frac{\sin^2\lambda}{\Delta\Omega_i} [\Omega_i (2\beta_{1i}$$

$$- \sin 2\beta_{1i}) + 4 \beta_{1i} \cos\beta_{1i} - 4 \sin\beta_{1i}]$$

$$+ \frac{16 \sin^2\lambda (1+\mu) \pi N}{\Delta\Omega \cos\lambda} \sum_{i=1}^{6N} Tm'i (\sin\beta_{1i} - \beta_{1i} \cos\beta_{1i})$$

$$Y_1 = Y_1 + \Delta Y_1 \quad \text{PRINT}$$

$$\Omega_0 = \Omega_0 + \Delta\Omega_0 \quad \text{PRINT}$$

CONTINUE

APPENDIX IV

EXPERIMENTAL SET-UP AND METHODS

In the first experiment (Figure 2.5) to measure the deflection of a free spring, a commercial auto spring with $h = 645$ mm, $r = 1.84$ mm, $\lambda = 85^\circ$ and $E = 2 \times 10^5$ N/mm² was used. In order to realize the theoretically assumed clamped end condition, one end of the spring was clamped between the two U-beams. The deflection of the free end was measured by means of a vernier scale.

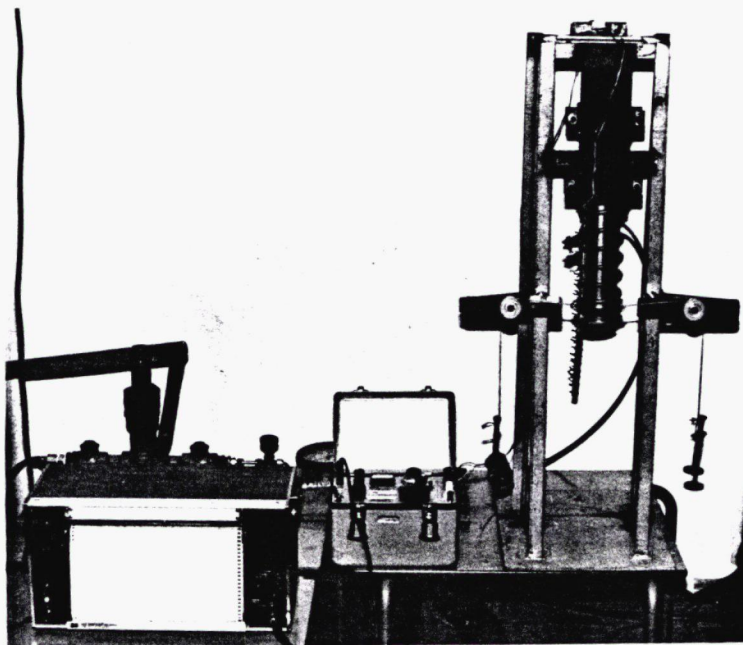


Figure (IV.1) Experimental Set-up.

In the second set of experiments to measure the rotation of free coils of the same spring, a mechanical Rotation Measuring Device (RMD) (Figure 3.7) was used. With the help of the strain gages attached on the two faces of a tiny beam clamped on one of the legs of the RMD, relative rotation of coils is measured in terms of the strain levels and recorded on a chart recorder. The spring was again clamped between two U-beams vertically on a rigid platform (Figure IV.1) and loading was slowly applied in small increments.